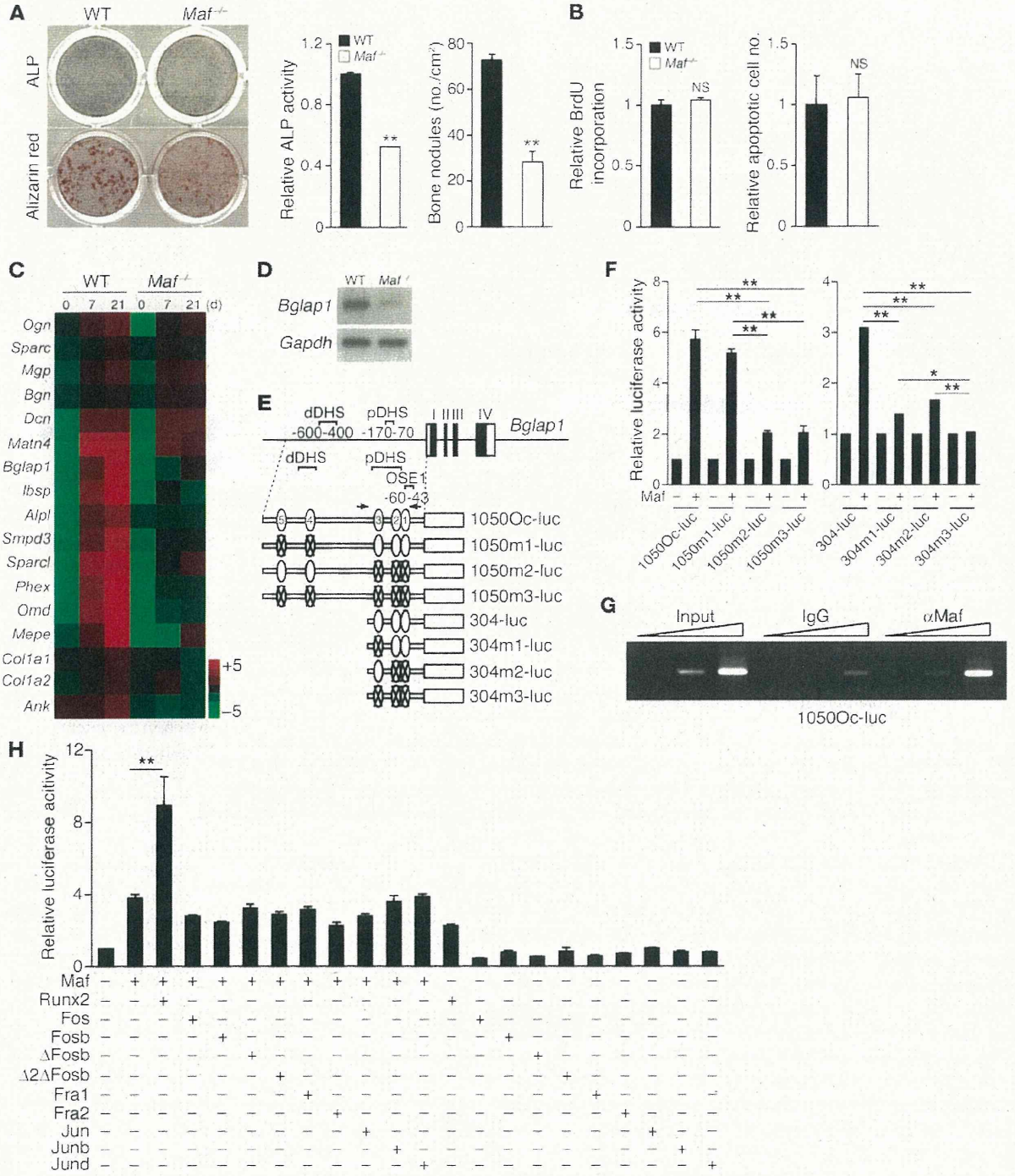

Figure 2

Regulation of osteoblast differentiation and *Bglap1* expression by Maf in cooperation with Runx2. (**A**) ALP and alizarin red staining of WT and *Maf*$^{-/-}$ calvarial cells. ALP activity and bone nodule formation were quantitated. (**B**) Proliferation and apoptosis of WT and *Maf*$^{-/-}$ calvarial cells. (**C**) mRNA expression of osteoblast-specific genes in WT and *Maf*$^{-/-}$ calvarial cells (GeneChip analysis). (**D**) *Bglap1* expression in WT and *Maf*$^{-/-}$ calvarial cells cultured with osteogenic medium for 7 days (RNA blot analysis). (**E**) Schematic of 5 MARE-like sequences (MARE1–MARE5) in the regulatory region of *Bglap1*, and *Bglap1*-luc variants harboring point mutation(s) in MARE-like sequences. pDHS and dDHS indicate proximal and distal DNase hypersensitive sites, respectively (23). Arrows indicate the primer set used for ChIP. Numbers within ovals represent corresponding MARE sequences. Ovals with "X"s indicate sequences without that respective MARE sequence. (**F**) Effect of Maf on the *Bglap1*-luc variants. (**G**) Recruitment of Maf to the *Bglap1* promoter region containing MARE1–MARE3. Calvarial cells cultured with osteogenic medium for 7 days were analyzed by ChIP. (**H**) Effect of Runx2 and AP-1 family members on Maf-mediated activation of 1050Oc-luc. $^{*}P < 0.05$; $^{**}P < 0.01$.

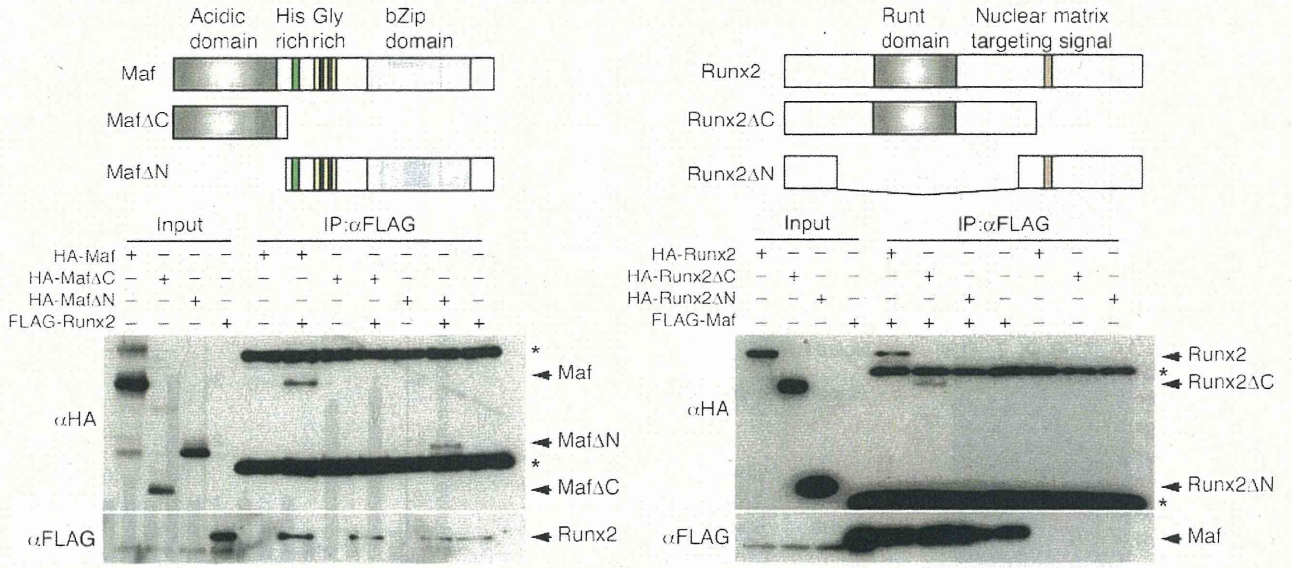

Figure 3

Physical interaction of Maf with Runx2. Maf and MafΔN, but not MafΔC, bound to Runx2. Runx2 and Runx2ΔC, but not Runx2ΔN, bound to Maf. Maf contains a transactivated domain (acidic domain), a histidine cluster (His rich), glycine stretches (Gly rich), and a basic leucine zipper domain (bZip domain). The asterisk indicates nonspecific bands.

DNA binding activity of Cebpδ, further supporting Maf-mediated inhibition of the *Pparg* promoter being independent of Maf binding to DNA (Supplemental Figure 16C). In addition, AP-1 family members and Runx2 did not affect Maf-mediated inhibition of the *Pparg* promoter (Supplemental Figure 16D). As it has been documented that Maf and Cebpδ commonly use CREB-binding protein gene (Crebbp) as their crucial transcriptional coactivator (29) (Supplemental Figure 8), we inferred that competition for the limited amount of Crebbp accounts for the inhibitory effect of Maf on the Cebpδ activity. As expected, the interaction of Cebpδ with Crebbp was suppressed by the overexpression of Maf (Figure 4F). Overexpression of Crebbp recovers the Maf-mediated inhibition of the effect of Cebpδ on the *Pparg* promoter (Figure 4E), lending support to the notion that Maf inhibits Cebpδ activity due to Crebbp squelching, although this may not be the sole mechanism underlying Maf inhibition of adipogenesis.

Decreased Maf expression accelerates age-related osteoporosis and fatty bone marrow. Although the perinatal lethality of *Maf*$^{-/-}$ mice renders it difficult to evaluate the development of fatty marrow with aging, the expression of *Pparg* in the bone marrow is much higher in perinatal *Maf*$^{-/-}$ mice than WT mice (Figure 5A), suggesting that the adipogenesis is enhanced in vivo in the case of *Maf* deficiency. Haploinsufficiency of *Maf* did not affect bone formation in embryos or neonatal mice (Figure 1B and Supplemental Figure 17). At the age of 22 weeks, however, histological analysis revealed that the bone marrow was filled with adipocytes characterized by fat vacuoles, and the bone volume was reduced in the *Maf*$^{+/-}$ mice (Figure 5, B and C, and Table 2). In contrast, no abnormalities in cartilage were found in the adult or neonatal *Maf*$^{+/-}$ mice (Supplemental Figures 6 and 18). The accelerated fatty marrow formation was accompanied by a decrease in osteoblast number and bone formation (Figure 5D), while osteoclastic bone resorption was not affected in the *Maf*$^{+/-}$ mice, with the serum calcium and phosphate levels being normally maintained (Supplemental Figures 19–21). Thus, haploinsufficiency of *Maf* results in enhanced adipogenesis and decreased osteogenesis in vivo, which was obvious at an advanced age, suggesting that the decreasing level of *Maf* with age contributes to the age-related switch in mesenchymal cell differentiation into adipocytes rather than osteoblasts.

To determine whether forced expression of Maf in mesenchymal cells would rescue an aging phenotype of *Maf*$^{+/-}$ mice, we overexpressed Maf in calvarial cells by retroviral transfer and transplanted them into the femurs of aged mice (Supplemental Figure 22). *Maf*$^{+/-}$ mice transplanted with Maf-transduced calvarial cells had a higher trabecular bone mass (but not cortical bone mass) and a decreased number of intramedullary adipocytes compared with those transplanted with mock-infected calvarial cells (Figure 6A and Table 3). We observed similar results when we transplanted Maf-transduced calvarial cells into aged WT mice (Supplemental Figure 22D). These results indicate that overexpression of Maf resulted in effective restoration of both an accelerated aging phenotype in *Maf*$^{+/-}$ mice and age-related changes in WT mice.

ROS regulation of Maf expression through Trp53. How is *Maf* expression regulated during aging? Since it has been reported that age-related bone loss is related to an increased expression of the Wnt inhibitor secreted frizzled-related protein 4 (30) or a decreased production of soluble factors, such as IGF1, TGFB1, IL-11, and bone morphogenetic protein 2 (6, 14, 15), we evaluated the effect of these factors as well as the effect of ROS on *Maf* expression. Although none of the soluble factors increased *Maf* expression in osteoblast precursor cells (Supplemental Figure 23), treatment with the hydrogen peroxide led to a marked decrease in *Maf* expression, which was restored by the addition of the antioxidant *N*-acetylcysteine (Figure 6B). These results prompted us to investigate whether administration of *N*-acetylcysteine rescue the bone phenotype of *Maf*$^{+/-}$ mice. As expected, administration of *N*-acetylcysteine led to an increased bone mass and decreased intramedullary fat in *Maf*$^{+/-}$ mice (Figure 6, C and D).

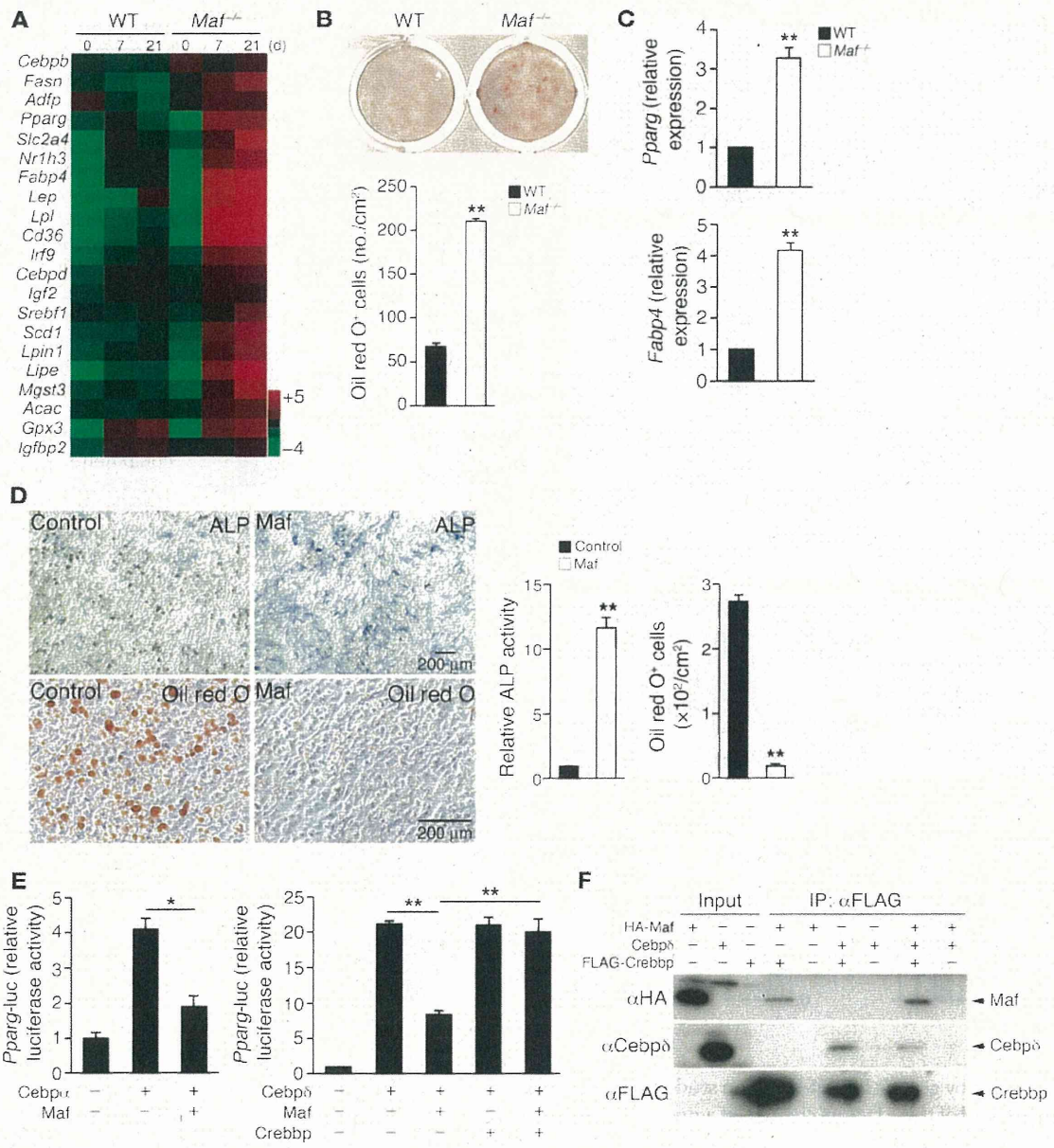

Figure 4

Maf inhibition of adipocyte differentiation by suppressing Cebpδ/α-mediated induction of *Pparg*. (**A**) mRNA expression of adipocyte-specific genes in WT and *Maf*$^{-/-}$ calvarial cells cultured with osteogenic medium (GeneChip analysis). (**B**) Adipocyte formation in WT and *Maf*$^{-/-}$ calvarial cells cultured with osteogenic medium (oil red O staining). (**C**) Expression of *Pparg* and *Fabp4* in WT and *Maf*$^{-/-}$ calvarial cells cultured with osteogenic medium (real-time RT-PCR analysis). (**D**) Effect of Maf overexpression on adipocyte and osteoblast differentiation of C3H10T1/2 cells. Scale bar: 200 μm. (**E**) Effect of Crebbp overexpression on Maf-mediated inhibition of Cebpδ activation of the *Pparg* promoter. (**F**) Inhibition of interaction between Cebpδ and Crebbp by Maf. $^{*}P < 0.05$; $^{**}P < 0.01$.

Furthermore, to gain mechanistic insight into the downregulation of *Maf* by ROS, we focused on the regulation of *Maf* by Trp53, which is reported to be induced by ROS and involved in aging (1, 2, 31, 32). Indeed, the *Maf* promoter contains multiple Trp53 binding sites and overexpression of Trp53 markedly inhibited the activity of the *Maf* promoter (Supplemental Figure 24). In addition, the downregulation of *Maf* by ROS was markedly attenuated in *Trp53*$^{-/-}$ osteoblasts (Figure 6B). Although NF-κB is involved in aging (33) and activated by ROS, *Maf* expression was not restored by an NF-κB inhibitor (Supplemental Figure 25). These results suggest that the oxidative stress that accumulates with aging mediates, at least in part, the age-related decrease in *Maf* expression through Trp53.

Discussion

The molecular basis for age-related changes in higher organisms is poorly understood, particularly in the skeletal system. Although many factors have been suggested to regulate the bifurcation of osteoblasts and adipocytes, the function of a few factors has been

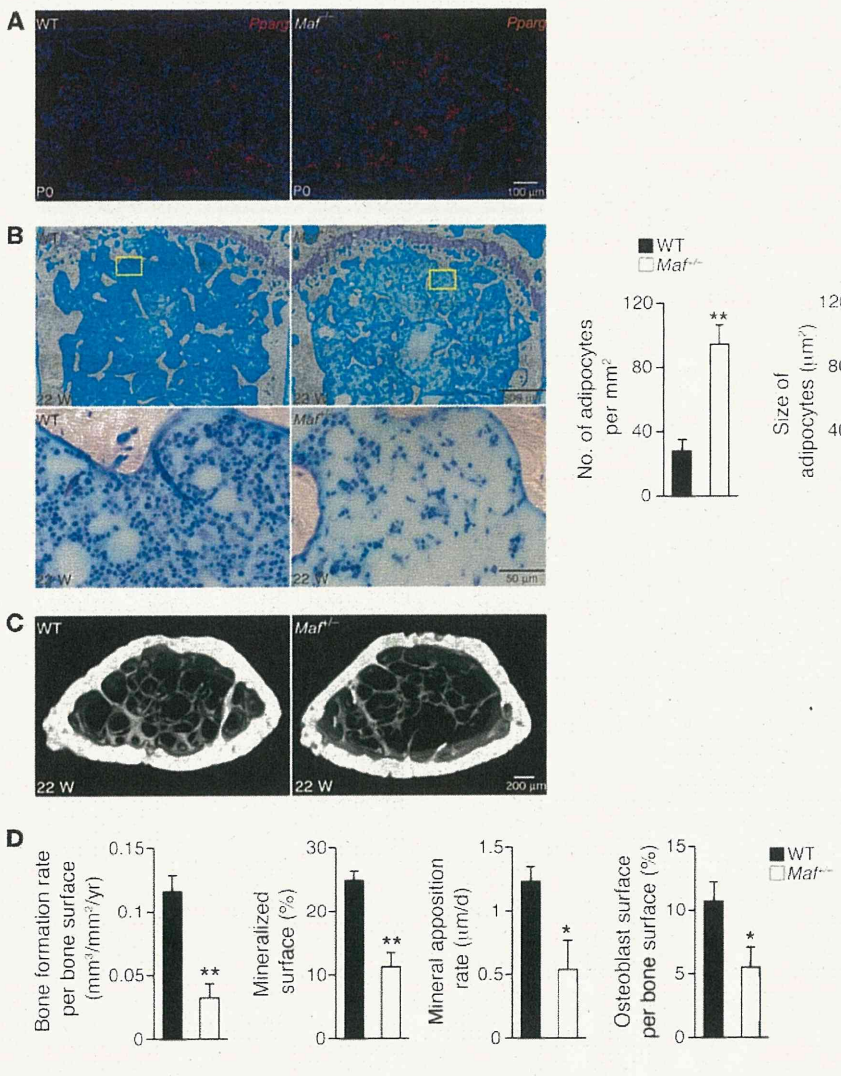

Figure 5
Increased adipogenesis in the *Maf* deficiency. (**A**) Expression of *Pparg* in the tibia of WT and *Maf*$^{-/-}$ littermates (in situ hybridization). Scale bar: 100 μm. (**B**) Histological analysis of the bone marrow of 22-week-old WT and *Maf*$^{+/-}$ female mice (femur, toluidine blue staining). Yellow boxed regions in the top panels are shown at higher magnification in the bottom panels. Note that *Maf*$^{+/-}$ bone marrow is filled with adipocytes. The number, but not the size, of adipocytes was significantly increased ($n = 6$). Scale bar: 500 μm (top row); 50 μm (bottom row). (**C**) Three-dimensional microcomputed tomography images of the femurs of 22-week-old WT and *Maf*$^{+/-}$ mice. Scale bar: 200 μm. (**D**) Parameters of osteoblastic bone formation in the bone morphometric analysis ($n = 6$; 22–26 weeks old). $^{*}P < 0.05$; $^{**}P < 0.01$.

demonstrated by genetic loss-of-function studies (7), and how the expression level of these factors changes in aging is not well known. A combination of a genome-wide screening and mouse genetic studies led us to identify the expression level of *Maf* to be both under the influence of aging and a determinant of mesenchymal cell differentiation into osteoblasts and adipocytes (Figure 6E).

Maf promotes osteoblast differentiation by regulating osteoblast genes, including *Bglap1*, in cooperation with Runx2. We propose that Maf functions as a modulator of bone formation by regulating the activity of crucial determinants like Runx2. Even in aged mice, bone marrow cells expressed a normal level of Runx2 (based on the screening shown in Figure 1A and Supplemental Table 1), but a low level of *Maf* expression resulted in a decrease in Runx2-mediated transcriptional activity. Therefore, Maf is a potential candidate to help explain the gradual and moderate decrease in bone formation observed in age-related osteoporosis. We also demonstrated that Maf inhibited adipocyte differentiation through the downregulation of *Pparg* expression, thus indicating that Maf regulates the bifurcation of the mesenchymal cell lineage into osteoblasts and adipocytes. It is interesting to note that the *MAF* locus was recently identified as one of the risk loci for obesity (34).

Using genetically modified mice, AP-1 superfamily members Fra1, Junb, and ΔFosb were shown to regulate bone formation (35–37), but ΔFosb was the only member that also regulates adipogenesis (19). However, since the adipogenic function of ΔFosb depends on a non–cell-autonomous mechanism (38), Maf is the only AP-1 superfamily member that has a cell-autonomous role in the regulation of both osteoblast and adipocyte differentiation. Interestingly, Maf also regulated osteoclastogenesis in a cell-autonomous manner, possibly by modulating NFAT activity (Sup-

Table 2
Skeletal development of 22-week-old *Maf*$^{+/-}$ mice

	WT	*Maf*$^{+/-}$
BV/TV (%)	4.43 ± 0.15	3.17 ± 0.54^{A}
Tb.N (mm^{-1})	1.90 ± 0.02	1.54 ± 0.14^{A}
Tb.Sp (μm)	503.82 ± 5.69	623.86 ± 51.19^{A}
Tb.Th (μm)	23.35 ± 0.59	20.98 ± 0.60^{A}

Microcomputed tomography analysis of the femurs of 22-week-old WT and *Maf*$^{+/-}$ mice. $^{A}P < 0.05$.

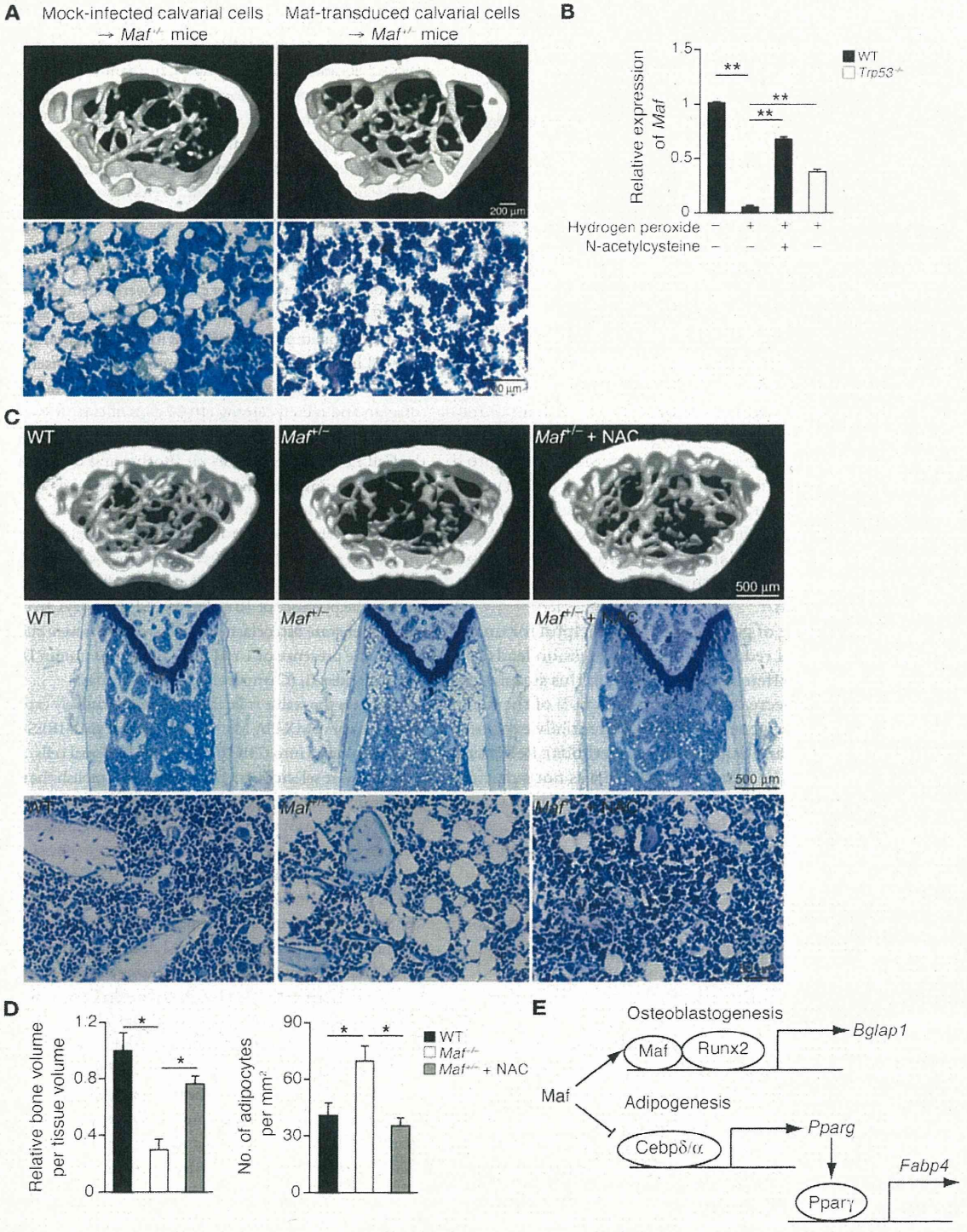

Figure 6

Aging and Maf-mediated regulation of osteoblastogenesis and adipogenesis. (**A**) Effect of Maf overexpression in mesenchymal cells on an aging phenotype of *Maf*$^{+/-}$ mice. Three-dimensional microcomputed tomography images and histological analysis of the bone marrow (toluidine blue staining) of *Maf*$^{+/-}$ mice transplanted with Maf-transduced or mock-infected calvarial cells. Scale bar: 200 μm (top row); 100 μm (bottom row). (**B**) Effect of hydrogen peroxide on *Maf* expression in WT and *Trp53*$^{-/-}$ calvarial osteoblasts (real-time RT-PCR analysis). (**C**) Effect of *N*-acetylcysteine (NAC) administration on an aging phenotype of *Maf*$^{+/-}$ mice. Three-dimensional microcomputed tomography images (top row) and histology of the bone marrow (toluidine blue staining, middle and bottom rows) of mice ($n = 4$). Images in the middle row are shown at higher magnification in the bottom row. Scale bar: 500 μm (top and middle rows); 50 μm (bottom row). (**D**) Microcomputed tomography and histological analysis of WT and *Maf*$^{+/-}$ mice. (**E**) A model of Maf-mediated reciprocal regulation of osteoblast and adipocyte differentiation. $^{*}P < 0.05$; $^{**}P < 0.01$.

Table 3
Skeletal development and adipogenesis in *Maf*$^{+/-}$ mice transplanted with Maf-transduced and mock-infected calvarial cells

	Mock-infected calvarial cells	Maf-transduced calvarial cells
BV/TV (%)	4.95 ± 0.77	6.81 ± 0.57[A]
CV/TV (%)	35.06 ± 0.43	35.09 ± 0.71
Adipocytes (mm^{-2})	97.1 ± 6.6	62.8 ± 6.7[B]

Effect of Maf overexpression in mesenchymal cells on an aging phenotype of *Maf*$^{+/-}$ mice (n = 4). CV/TV, cortical bone volume/total volume. [A]$P < 0.05$. [B]$P < 0.01$.

plemental Figure 5, C and E), suggesting that Maf plays a distinct role in each skeletal cell type.

Since Pparγ inhibits the expression of *Maf* (39), a small reduction in *Maf* expression would form a vicious cycle: an increasing expression of *Pparg* further inhibits *Maf* expression, leading to a severe reduction in *Maf*. Antidiabetic drugs — such as TZDs, which activate Pparγ — are known to reduce bone mass and increase fracture risk (12). Interestingly, treatment with rosiglitazone led to decreased *Maf* expression (data not shown). This is possibly because Pparγ agonists accelerate this vicious cycle through suppression of *Maf* expression.

Mathematical modeling of gene expression is helpful for understanding how the gradual reduction of *Maf* expression leads to a dramatic change in cell differentiation. Based on this simulation, if the expression of *Maf* decreased by more than 60% of the maximum level, the adipogenic genes became preferentially expressed (Supplemental Figure 26 and Supplemental Methods). Reduction of *Maf* gene expression in neonatal *Maf*$^{+/-}$ mice was not sufficient for activation of this switch, as we observed no obvious bone phenotype in neonatal *Maf*$^{+/-}$ mice (Figure 1B and Supplemental Figure 17). As the level of *Maf* gradually decreased with age, they exhibited an osteopenic phenotype with fatty marrow.

Currently, there are few drugs available in the clinic that effectively increase bone formation. The modulation of *Maf* expression appears to hold considerable promise as what we believe to be a novel antiaging therapeutic target in the skeletal system.

Methods

Mice. Maf$^{-/-}$ mice were previously generated and described elsewhere (16). *Maf*$^{-/-}$ mice were backcrossed into C57BL/6 mice for more than 9 generations, unless otherwise described. All mice were born and maintained under specific pathogen–free conditions. All animal experiments were performed with the approval of the Animal Study Committee of Tokyo Medical and Dental University and conformed to relevant guidelines and laws.

Microcomputed tomography analysis. CT scanning was performed using a ScanXmate-A100S Scanner (Comscantechno). Three-dimensional microstructural image data were reconstructed and structural indices were calculated using TRI/3D-BON software (RATOC). Bone mineral density (BMD) was calculated using TRI/3D-BON-BMD-PNTM software (RATOC). Bone morphometric and BMD analyses were performed at a region 0.8–1.8 mm above the distal growth plate of the femur in adult mice and using the full-length femur in postnatal mice, unless otherwise described.

In situ hybridization and immunohistochemical analysis. Embryos and bones were fixed in 4% paraformaldehyde, embedded in paraffin, and sectioned (5 μm). In situ hybridization was performed using ^{35}S-labeled *Bglap1*, *Runx2*, and *Col1a1* probes as described previously (40). The *Pparg* probe is a 521-bp fragment of the *Pparg* coding region. Immunohistochemical analysis was performed using a standard avidin-biotin peroxidase method (Vector Laboratories), according to the manufacturer's protocols. Paraffin-embedded sections were dewaxed, rehydrated, and subjected to an antigen retrieval procedure. The sections were then blocked with 5% lamb serum and incubated with the antibody. The antibodies are listed in Supplemental Table 2. For the proliferation assay, pregnant mice were injected with BrdU 1 hour before sacrifice. We detected mitotic cells using the BrdU Staining Kit (Zymed) and detected apoptotic cells by TUNEL staining with the ApoAlert DNA Fragmentation Kit (Clontech).

Cell cultures. For in vitro osteoblast and adipocyte differentiation, cells derived from bone marrow or calvaria were cultured with osteogenic medium (50 μM ascorbic acid, 10 nM dexamethasone, and 10 mM β-glycerophosphate) or adipogenic medium (0.5 mM 3-isobutyl-1-methylxanthine, 5 μg/ml insulin, and 1 μM dexamethasone), as described previously (20, 41). ALP assay (7 days of culture), alizarin red staining (21 days of culture), and oil red O staining (10 days of culture) were performed as previously described (20, 41). We determined the rate of cell proliferation using the Cell Proliferation ELISA kit (Roche) and detected apoptotic cells by TUNEL staining with the MEBSTATIN Apoptosis Kit Direct (MBL). The method for in vitro osteoclast differentiation was described previously (42–44). Briefly, bone marrow–, fetal liver–, or spleen-derived cells, cultured with 10 ng/ml M-CSF (R&D Systems) for 2 days, were used as osteoclast precursor cells, which were further cultured with 50 ng/ml RANKL (Peprotech) in the presence of 10 ng/ml M-CSF for 3 days. In the coculture system used to generate osteoclasts, bone marrow cells were cultured with calvarial cells in the presence of 1 nM 1,25-dihydroxyvitamin D_3 (Wako) and 1 μM prostaglandin E_2 (Cayman Chemical) for 7 days.

To obtain the stable transformants constitutively expressing Maf, the retroviral vectors pMX-HA-Maf-IRES-Puro and pMX-IRES-Puro, as the control, were introduced into C3H10T1/2 and ST2 clonal cells, and the stable transformants were selected with puromycin. To establish the stable transformants expressing shRNAs targeting Maf, the retroviral vectors pSIREN-shMaf and pSIREN-shControl were introduced into ST2 clonal cells, and stable transformants were selected with puromycin. For osteoblast and adipocyte differentiation, transformants were cultured under an osteogenic condition (50 μM ascorbic acid, 10 nM dexamethasone, 10 mM β-glycerophosphate, and 100 ng/ml BMP2) and adipogenic condition (0.26 mM 3-isobutyl-1-methylxanthine, 85 nM insulin, and 0.5 μM dexamethasone), respectively.

Transplantation of Maf-transduced calvarial cells. The transplantation experiment was performed as described previously (45) with minor modifications. Briefly, we used 32-week-old WT and *Maf*$^{+/-}$ mice as recipients and newborn *Maf*$^{+/-}$ mice as donors. The mice were obtained from an intercross between *Maf*$^{+/-}$ mice, which are backcrossed into C57BL/6 mice for more than 9 generations. The mice were anesthetized by an injection of somnopentyl into the peritoneal cavity, and the proximal femur was gently drilled with a diamond-coated burr. Cells were obtained from calvaria derived from newborn *Maf*$^{+/-}$ mice and transduced with a retroviral vector (pMX-HA-Maf-IRES-GFP or pMX-IRES-GFP). The Maf-transduced or mock-infected calvarial cells were directly injected into the bone marrow cavity through the hole in the femur using a 28-gauge needle (approximately 1×10^5 cells per femur). The needle was inserted almost to the distal metaphysis. After transplantation, the drilled hole was filled with bone cement (Fuji Lute, GC). The mice were analyzed 1 month after transplantation. Microcomputed tomography analysis and measurement of fat marrow were performed within 1 mm above the distal growth plate of the femur.

Administration of N-acetylcysteine. Maf$^{+/-}$ mice were backcrossed into C57BL/6 mice for more than 3 generations. Mice were supplied drinking water containing 2 mg/ml *N*-acetylcysteine ad libitum for 14 weeks. At 22 weeks of age, mice were sacrificed and analyzed.

RNA blot and real-time RT-PCR analyses. Total RNA was extracted with ISOGEN (Wako) or the RNeasy Lipid Tissue Mini Kit (Qiagen). Total RNA was blotted and hybridized with [α-^{32}P]dCTP-labeled probes for *Maf*, *Bglap1*, and *Gapdh*, as described previously (39, 41). Real-time RT-PCR was performed with a LightCycler (Roche) using SYBR Green (Toyobo) as described previously (44). The primer sequences are listed in Supplemental Table 3.

GeneChip analysis. GeneChip analysis, clustering analysis, and GSEA were performed as described previously (42, 46, 47). Calvarial cells cultured with osteogenic medium for 0, 7, and 21 days were analyzed. BMSCs derived from 8- and 32-week-old mice were isolated as described previously (48) with minor modifications. Briefly, bone marrow cells from each of the mice were isolated by flushing the femurs and tibiae with α-MEM with 10% FBS, and these cells were plated on plastic dishes. After 3 days, adherent cells were used. BMSCs contain a precursor of osteoblasts and adipocytes (data not shown) (49). The total RNAs extracted from these cells were used for cDNA synthesis by reverse transcription, followed by synthesis of biotinylated cRNA through in vitro transcription. After cRNA fragmentation, hybridization with the Mouse Genome 430 2.0 Array (Affymetrix) was performed as described previously (42). The main part of the data set was deposited and can be obtained from the Genome Network Platform (http://genomenetwork.nig.ac.jp/).

ChIP assay. After calvarial cells were cultured with osteogenic medium for 7 days, ChIP assay was performed using the ChIP Assay Kit (Upstate) with minor modification. The antibodies used are listed in Supplemental Table 2. The primer sequences are listed in Supplemental Table 3.

Retroviral gene transfer. Retroviral vectors pMX-HA-Maf-IRES-GFP and pMX-HA-Maf-IRES-Puro were constructed by inserting DNA fragments encoding HA and Maf into pMX-IRES-GFP and pMX-IRES-Puro (50). Retroviral vectors pSIREN-shMaf and pSIREN-shControl were constructed by inserting annealed oligonucleotide into RNAi-Ready pSIREN-RetroQ (BD Biosciences). The oligonucleotide sequences are listed in Supplemental Table 3. Retroviral packaging was performed by transfecting the plasmids into Plat-E or Plat-A cells using FuGENE6 as described previously (50).

Reporter gene assay. The reporter plasmids, *Bglap1*-luc variants, were constructed from 1050Oc-luc (41), and mutations in MARE-like sequences were introduced by PCR. A site-directed mutagenesis performed with sequential PCR steps was used to engineer the mutated MARE-like sequences. Two overlapping PCR fragments, each containing the MARE1–MARE5 mutation, were generated. The corresponding PCR fragments were used as templates for the second PCR step. The primer sequences are listed in Supplemental Table 3. *Maf*-luc was constructed by subcloning a 2-kb fragment of the 5′ flanking region of the *Maf* gene into the pGL3-basic vector (Promega). Luciferase assay was performed in NIH3T3 cells or mouse embryonic fibroblasts (MEFs) established from WT and *Runx2*$^{-/-}$ E14 embryos (51). *Pparg*-luc was constructed by subcloning a 2.2-kb fragment of the 5′ flanking region of the *Pparg* gene (52) into the pGL3-basic vector, and mutations in MAREs were introduced by PCR. The primer sequences are listed in Supplemental Table 3. Luciferase assay was performed in 3T3-L1 cells. The expression plasmids of Maf, Runx2, Fos, Fosb, Fosl1, Fosl2, Jun, Junb, Jund, Cebpα, Cebpβ, Cebpδ, Crebbp, p50, p65, and Tp53 have been described elsewhere (16, 41, 42, 53–58). The expression plasmids of ΔFosb and Δ2ΔFosb were constructed from full-length Fosb cDNA using PCR. The reporter plasmids (p*Acp5*-luc, ref. 42, and p*Nfatc1*-luc, ref. 43) were described previously. MEFs and NIH3T3 and 3T3-L1 cells were transfected using Lipofectamine plus reagents (Invitrogen). After 30–36 hours, dual luciferase assay was performed according to the manufacturer's protocols (Promega).

Immunoblot and immunoprecipitation analyses. Immunoblot and immunoprecipitation analyses were performed as previously described (59). The antibodies used are listed in Supplemental Table 2. For analyzing the interaction between Maf and Runx2, HA-tagged Maf, HA-tagged N-terminal region of Maf (HA-tagged MafΔC), HA-tagged C-terminal region of Maf (HA-tagged MafΔN), HA-tagged Runx2, HA-tagged Runx2ΔN, HA-tagged Runx2ΔC, FLAG-tagged Maf, and FLAG-tagged Runx2 proteins were produced by the in vitro transcription/translation system (Promega). These proteins were mixed in a binding buffer and incubated with anti-FLAG antibody-conjugated agarose beads (Sigma-Aldrich). Recovered proteins were subjected to immunoblot analysis with anti-FLAG and anti-HA antibodies. For analyzing the interaction among Maf, Cebpδ, and Crebbp, HA-tagged Maf and Cebpδ proteins were produced by the in vitro transcription/translation system. FLAG-tagged Crebbp proteins were produced by transfecting FLAG-Crebbp expression plasmids into HEK293T cells using FuGENE6 (Roche). These proteins were mixed and incubated with anti-FLAG antibody-conjugated agarose beads. Recovered proteins were subjected to immunoblot analysis with anti-Cebpδ, anti-FLAG, and anti-HA antibodies.

Treatment of Trp53$^{-/-}$ *osteoblasts with hydrogen peroxide.* Osteoblasts were isolated from the calvaria of newborn mice deficient in *Trp53* (accession no., CDB0001K; http://www.cdb.riken.jp/arg/mutant%20mice%20list.html) (60) and treated with 600 μM hydrogen peroxide. Five days after the treatment, mRNAs were extracted and subjected to real-time PCR analysis.

EMSA. EMSA was performed as previously described (59). Maf and Cebpδ proteins were produced by the in vitro transcription/translation system. The CCAAT probe for binding of Cebpδ and the MARE probe for binding of Maf were generated by annealing synthetic oligonucleotides. The oligonucleotide sequences are listed in Supplemental Table 3. Antibodies against Maf and Cebpδ were used for supershift analysis.

ELISA. Soluble osteocalcin levels and TRAP activity in serum were detected using the mouse osteocalcin EIA kit (Biomedical Technologies Inc.) and mouse TRAP assay (SBA Sciences), respectively.

Statistics. Statistical analysis was performed using Student's *t* test for comparisons between 2 groups and analysis of variance with Bonferroni post-hoc test for comparisons among 3 or more groups, unless otherwise described. All data are expressed as mean ± SEM.

Acknowledgments

We thank H.R. Ueda, M. Asagiri, T. Ando, Y. Kunisawa, T. Honda, Y. Suzuki, T. Kudo, A. Izumi, A. Suematsu, and A. Hirota for discussion and assistance. This work was supported in part by a grant for ERATO from the Takayanagi Osteonetwork Project from the Japan Science and Technology Agency; Grant-in-Aids for Creative Scientific Research and Young Scientist (A and Start-up) from the Japan Society for the Promotion of Science (JSPS); Grant-in-Aid for Challenging Exploratory Research JSPS; grants for the Genome Network Project and Global Center of Excellence Program from the Ministry of Education, Culture, Sports, Science and Technology of Japan; and grants from Tokyo Biochemical Research Foundation, Life Science Foundation of Japan, Yokoyama Foundation for Clinical Pharmacology, and Takeda Science Foundation.

Received for publication February 1, 2010, and accepted in revised form July 14, 2010.

Address correspondence to: Hiroshi Takayanagi, Department of Cell Signaling, Graduate School of Medical and Dental Sciences, Tokyo Medical and Dental University, Yushima 1-5-45, Bunkyo-ku, Tokyo 113-8549, Japan. Phone: 81.3.5803.5471; Fax: 81.3.5803.0192; E-mail: taka.csi@tmd.ac.jp.

1. Collado M, Blasco MA, Serrano M. Cellular senescence in cancer and aging. *Cell.* 2007;130(2):223–233.
2. Chen JH, Hales CN, Ozanne SE. DNA damage, cellular senescence and organismal ageing: causal or correlative? *Nucleic Acids Res.* 2007;35(22):7417–7428.
3. Uccelli A, Moretta L, Pistonia V. Mesenchymal stem cells in health and disease. *Nat Rev Immunol.* 2008;8(9):726–736.
4. Engler AJ, Sen S, Sweeney HL, Discher DE. Matrix elasticity directs stem cell lineage specification. *Cell.* 2006;126(4):677–689.
5. Meunier P, Aaron J, Edouard C, Vignon G. Osteoporosis and the replacement of cell populations of the marrow by adipose tissue. A quantitative study of 84 iliac bone biopsies. *Clin Orthop Relat Res.* 1971; 80:147–154.
6. Manolagas SC. Birth and death of bone cells: basic regulatory mechanisms and implications for the pathogenesis and treatment of osteoporosis. *Endocr Rev.* 2000;21(2):115–137.
7. Gimble JM, Zvonic S, Floyd ZE, Kassem M, Nuttall ME. Playing with bone and fat. *J Cell Biochem.* 2006;98(2):251–266.
8. Belaid-Choucair Z, et al. Human bone marrow adipocytes block granulopoiesis through neuropilin-1-induced granulocyte colony-stimulating factor inhibition. *Stem Cells.* 2008;26(6):1556–1564.
9. Corre J, Planat-Benard V, Corberand JX, Penicaud L, Casteilla L, Laharrague P. Human bone marrow adipocytes support complete myeloid and lymphoid differentiation from human CD34 cells. *Br J Haematol.* 2004;127(3):344–347.
10. Maurin AC, Chavassieux PM, Frappart L, Delmas PD, Serre CM, Meunier PJ. Influence of mature adipocytes on osteoblast proliferation in human primary cocultures. *Bone.* 2000;26(5):485–489.
11. Naveiras O, Nardi V, Wenzel PL, Hauschka PV, Fahey F, Daley GQ. Bone-marrow adipocytes as negative regulators of the haematopoietic microenvironment. *Nature.* 2009;460(7252):259–263.
12. McDonough AK, Rosenthal RS, Cao X, Saag KG. The effect of thiazolidinediones on BMD and osteoporosis. *Nat Clin Pract Endocrinol Metab.* 2008; 4(9):507–513.
13. Seeman E, Delmas PD. Bone quality--the material and structural basis of bone strength and fragility. *N Engl J Med.* 2006;354(21):2250–2261.
14. Lamberts SW, van den Beld AW, van der Lely AJ. The endocrinology of aging. *Science.* 1997; 278(5337):419–424.
15. Rosen CJ. Growth hormone, insulin-like growth factors, and the senescent skeleton: Ponce de Leon's Fountain revisited? *J Cell Biochem.* 1994; 56(3):348–356.
16. Kawauchi S, et al. Regulation of lens fiber cell differentiation by transcription factor c-Maf. *J Biol Chem.* 1999;274(27):19254–19260.
17. Ho IC, Glimcher LH. Transcription: tantalizing times for T cells. *Cell.* 2002;109 suppl:S109–S120.
18. MacLean HE, Kim JI, Glimcher MJ, Wang J, Kronenberg HM, Glimcher LH. Absence of transcription factor c-maf causes abnormal terminal differentiation of hypertrophic chondrocytes during endochondral bone development. *Dev Biol.* 2003;262(1):51–63.
19. Sabatakos G, et al. Overexpression of DeltaFosB transcription factor(s) increases bone formation and inhibits adipogenesis. *Nat Med.* 2000;6(9):985–990.
20. Hong JH, et al. TAZ, a transcriptional modulator of mesenchymal stem cell differentiation. *Science.* 2005;309(5737):1074–1078.
21. Karsenty G, Wagner EF. Reaching a genetic and molecular understanding of skeletal development. *Dev Cell.* 2002;2(4):389–406.
22. Yang X, et al. ATF4 is a substrate of RSK2 and an essential regulator of osteoblast biology; implication for Coffin-Lowry Syndrome. *Cell.* 2004; 117(3):387–398.
23. Montecino M, Lian J, Stein G, Stein J. Changes in chromatin structure support constitutive and developmentally regulated transcription of the bone-specific osteocalcin gene in osteoblastic cells. *Biochemistry.* 1996;35(15):5093–5102.
24. Lee CH, Olson P, Evans RM. Minireview: lipid metabolism, metabolic diseases, and peroxisome proliferator-activated receptors. *Endocrinology.* 2003; 144(6):2201–2207.
25. Farmer SR. Transcriptional control of adipocyte formation. *Cell Metab.* 2006;4(4):263–273.
26. Tontonoz P, Spiegelman BM. Fat and beyond: the diverse biology of PPARgamma. *Annu Rev Biochem.* 2008;77:289–312.
27. Shi XM, Blair HC, Yang X, McDonald JM, Cao X. Tandem repeat of C/EBP binding sites mediates PPARgamma2 gene transcription in glucocorticoid-induced adipocyte differentiation. *J Cell Biochem.* 2000;76(3):518–527.
28. Wu Z, et al. Cross-regulation of C/EBP alpha and PPAR gamma controls the transcriptional pathway of adipogenesis and insulin sensitivity. *Mol Cell.* 1999;3(2):151–158.
29. Kovacs KA, Steinmann M, Magistretti PJ, Halfon O, Cardinaux JR. CCAAT/enhancer-binding protein family members recruit the coactivator CREB-binding protein and trigger its phosphorylation. *J Biol Chem.* 2003;278(38):36959–36965.
30. Nakanishi R, et al. Secreted frizzled-related protein 4 is a negative regulator of peak BMD in SAMP6 mice. *J Bone Miner Res.* 2006;21(11):1713–1721.
31. Almeida M, et al. Skeletal involution by age-associated oxidative stress and its acceleration by loss of sex steroids. *J Biol Chem.* 2007;282(37):27285–27297.
32. Tyner SD, et al. p53 mutant mice that display early ageing-associated phenotypes. *Nature.* 2002; 415(6867):45–53.
33. Adler AS, Sinha S, Kawahara TL, Zhang JY, Segal E, Chang HY. Motif module map reveals enforcement of aging by continual NF-kappaB activity. *Genes Dev.* 2007;21(24):3244–3257.
34. Meyre D, et al. Genome-wide association study for early-onset and morbid adult obesity identifies three new risk loci in European populations. *Nat Genet.* 2009;41(2):157–159.
35. Jochum W, et al. Increased bone formation and osteosclerosis in mice overexpressing the transcription factor Fra-1. *Nat Med.* 2000;6(9):980–984.
36. Eferl R, et al. The Fos-related antigen Fra-1 is an activator of bone matrix formation. *EMBO J.* 2004; 23(14):2789–2799.
37. Kenner L, et al. Mice lacking JunB are osteopenic due to cell-autonomous osteoblast and osteoclast defects. *J Cell Biol.* 2004;164(4):613–623.
38. Rowe GC, Choi CS, Neff L, Horne WC, Shulman GI, Baron R. Increased energy expenditure and insulin sensitivity in the high bone mass DeltaFosB transgenic mice. *Endocrinology.* 2009;150(1):135–143.
39. Serria MS, Ikeda H, Omoteyama K, Hirokawa J, Nishi S, Sakai M. Regulation and differential expression of the c-maf gene in differentiating cultured cells. *Biochem Biophys Res Commun.* 2003; 310(2):318–326.
40. Takeda S, Bonnamy JP, Owen MJ, Ducy P, Karsenty G. Continuous expression of Cbfa1 in nonhypertrophic chondrocytes uncovers its ability to induce hypertrophic chondrocyte differentiation and partially rescues Cbfa1-deficient mice. *Genes Dev.* 2001; 15(4):467–481.
41. Kim S, et al. Stat1 functions as a cytoplasmic attenuator of Runx2 in the transcriptional program of osteoblast differentiation. *Genes Dev.* 2003; 17(16):1979–1991.
42. Takayanagi H, et al. Induction and activation of the transcription factor NFATc1 (NFAT2) integrate RANKL signaling in terminal differentiation of osteoclasts. *Dev Cell.* 2002;3(6):889–901.
43. Asagiri M, et al. Autoamplification of NFATc1 expression determines its essential role in bone homeostasis. *J Exp Med.* 2005;202(9):1261–1269.
44. Nishikawa K, et al. Blimp1-mediated repression of negative regulators is required for osteoclast differentiation. *Proc Natl Acad Sci U S A.* 2010; 107(7):3117–3122.
45. Zhang XS, et al. Local ex vivo gene therapy with bone marrow stromal cells expressing human BMP4 promotes endosteal bone formation in mice. *J Gene Med.* 2004;6(1):4–15.
46. Eisen MB, Spellman PT, Brown PO, Botstein D. Cluster analysis and display of genome-wide expression patterns. *Proc Natl Acad Sci U S A.* 1998; 95(25):14863–14868.
47. Subramanian A, et al. Gene set enrichment analysis: a knowledge-based approach for interpreting genome-wide expression profiles. *Proc Natl Acad Sci U S A.* 2005;102(43):15545–15550.
48. Xiao Y, Fu H, Prasadam I, Yang YC, Hollinger JO. Gene expression profiling of bone marrow stromal cells from juvenile, adult, aged and osteoporotic rats: with an emphasis on osteoporosis. *Bone.* 2007;40(3):700–715.
49. Holmes C, Khan TS, Owen C, Ciliberti N, Grynpas MD, Stanford WL. Longitudinal analysis of mesenchymal progenitors and bone quality in the stem cell antigen-1-null osteoporotic mouse. *J Bone Miner Res.* 2007;22(9):1373–1386.
50. Morita S, Kojima T, Kitamura T. Plat-E: an efficient and stable system for transient packaging of retroviruses. *Gene Ther.* 2000;7(12):1063–1066.
51. Otto F, et al. Cbfa1, a candidate gene for cleidocranial dysplasia syndrome, is essential for osteoblast differentiation and bone development. *Cell.* 1997;89(5):765–771.
52. Kudo M, Sugawara A, Uruno A, Takeuchi K, Ito S. Transcription suppression of peroxisome proliferator-activated receptor gamma2 gene expression by tumor necrosis factor alpha via an inhibition of CCAAT/ enhancer-binding protein delta during the early stage of adipocyte differentiation. *Endocrinology.* 2004;145(11):4948–4956.
53. Nishiyori A, et al. Determination of tissue specificity of the enhancer by combinatorial operation of tissue-enriched transcription factors. Both HNF-4 and C/EBP beta are required for liver-specific activity of the ornithine transcarbamylase enhancer. *J Biol Chem.* 1994;269(2):1323–1331.
54. Matsuo K, Owens JM, Tonko M, Elliott C, Chambers TJ, Wagner EF. Fosl1 is a transcriptional target of c-Fos during osteoclast differentiation. *Nat Genet.* 2000;24(2):184–187.
55. Ohoka N, Yoshii S, Hattori T, Onozaki K, Hayashi H. TRB3, a novel ER stress-inducible gene, is induced via ATF4-CHOP pathway and is involved in cell death. *EMBO J.* 2005;24(6):1243–1255.
56. Kawai J, et al. Functional annotation of a full-length mouse cDNA collection. *Nature.* 2001; 409(6821):685–690.
57. Koga T, et al. NFAT and Osterix cooperatively regulate bone formation. *Nat Med.* 2005;11(8):880–885.
58. Tanikawa J, et al. p53 suppresses the c-Myb-induced activation of heat shock transcription factor 3. *J Biol Chem.* 2000;275(20):15578–15585.
59. Nishikawa K, et al. Self-association of Gata1 enhances transcriptional activity in vivo in zebra fish embryos. *Mol Cell Biol.* 2003;23(22):8295–8305.
60. Tsukada T, et al. Enhanced proliferative potential in culture of cells from p53-deficient mice. *Oncogene.* 1993;8(12):3313–3322.

Histopathology 2011, **58**, 531–542. DOI: 10.1111/j.1365-2559.2011.03759.x

Down-regulation of keratin 4 and keratin 13 expression in oral squamous cell carcinoma and epithelial dysplasia: a clue for histopathogenesis

Kei Sakamoto,[1] Tadanobu Aragaki,[2] Kei-ichi Morita,[3] Hiroshi Kawachi,[4] Kou Kayamori,[1] Shoichi Nakanishi,[1] Ken Omura,[3] Yoshio Miki,[5,6] Norihiko Okada,[7] Ken-ichi Katsube,[1] Toichiro Takizawa[8] & Akira Yamaguchi[1]

Sections of [1]Oral Pathology, [2]Maxillofacial Surgery, [3]Oral and Maxillofacial Surgery, [4]Human Pathology, Graduate School, Tokyo Medical and Dental University, [5]Section of Molecular Genetics, Medical Research Institute, Tokyo Medical and Dental University, [6]Department of Genetic Diagnosis, Cancer Institute, Japanese Foundation for Cancer Research, [7]Section of Diagnostic Oral Pathology, Graduate School, Tokyo Medical and Dental University, and [8]Section of Molecular Pathophysiology, Graduate School of Allied Health Sciences, Tokyo Medical and Dental University, Tokyo, Japan

Date of submission 10 July 2009
Accepted for publication 26 April 2010

Sakamoto K, Aragaki T, Morita K-i, Kawachi H, Kayamori K, Nakanishi S, Omura K, Miki Y, Okada N, Katsube K-i, Takizawa T & Yamaguchi A
(2011) *Histopathology* **58**, 531–542

Down-regulation of keratin 4 and keratin 13 expression in oral squamous cell carcinoma and epithelial dysplasia: a clue for histopathogenesis

Aims: This study aimed to identify relevant keratin subtypes that may associate with the pathogenesis of oral epithelial neoplasms.
Methods and results: Expression of all the keratin subtypes was examined by cDNA microarray analysis of 43 oral squamous cell carcinoma (OSCC) cases. Immunohistochemical expression of the major keratins was examined in 100 OSCC and oral epithelial dysplasia (OED) cases. Many changes in keratin expression were observed and, significantly, consistent down-regulation of keratin 4 (K4) and K13 expression was observed. Aberrant expression of K4 and K13 was associated with morphological changes in the affected oral epithelium. Experiments with cell cultures transfected with various keratin subtypes suggested that alterations in keratin subtype expression can cause changes in cell shape and movement.
Conclusions: Aberrant expression of K4 and K13, which are the dominant pair of differentiation-related keratins in oral keratinocytes, indicates dysregulation of epithelial differentiation in OSCC and OED. These keratins, especially K4, may be useful for pathological diagnosis. We propose that the aberrant expression of K4 and K13 and concomitant up-regulation of the other keratins may be one of the causative factors for morphological alterations in the affected epithelium.

Keywords: cytokeratin, epithelial dysplasia, keratin, keratin 4, keratin 13, oral mucosa, squamous cell carcinoma

Abbreviations: EDTA, Tris/ethylenediamine tetraacetic acid; OED, oral epithelial dysplasia; OSCC, oral squamous cell carcinoma; SCC, squamous cell carcinoma

Introduction

Keratin is an intermediate filament cytoskeletal protein. The human genome contains 54 genes encoding functional keratins, of which 37 encode epithelial keratins and 17 encode hair keratins. Keratins can be divided into acidic and basic types; both types are coexpressed during the differentiation of epithelial tissues and arranged in heterotypic pairs to form chains of laterally aligned coiled-coil structure.[1] Because the composition

Address for correspondence: K Sakamoto, Section of Oral Pathology, Tokyo Medical and Dental University, Yushima 1-5-45, Bunkyo-ku, Tokyo 113-0034, Japan. e-mail: s-kei.mpa@tmd.ac.jp

of keratin pairs varies depending on cell type, differentiation status and environment, the assessment of the distribution of different keratin subtypes can facilitate cell typing and identification. Moreover, keratin subtyping is useful for cancer diagnosis, as cancer cells often exhibit abnormal keratin expression profiles.[1]

Several studies have indicated that some specific keratin subtypes are either down-regulated or up-regulated in oral squamous cell carcinoma (OSCC) and oral epithelial dysplasia (OED).[2–17] However, these studies have investigated limited numbers of selective keratin subtypes, and hence the results of different studies are often conflicting; this is probably because of the variations in the experimental procedures used, including the use of different antibodies. The correlation of each keratin subtype and its significance in pathogenesis has not been assessed fully.

In this study, we performed exhaustive keratin profiling to elucidate the comprehensive alterations in the expression of keratin subtypes in OSCC and OED.

Materials and methods

CLINICAL SPECIMENS

The surgical specimens from 43 patients with OSCC were collected for microarray analysis. The primary sites of cancer were tongue (18), gingiva (16), oral floor (five), buccal mucosa (three) and palate (one). Written informed consent was obtained from all the patients, and all the experimental procedures were approved by the Tokyo Medical and Dental University ethics committee. In addition, 100 specimens of OSCC and OED that were large enough to be sufficiently informative and contained normal epithelium were collected from the archives of the Dental Hospital at Tokyo Medical and Dental University. Grading of OED was performed according to the generally accepted criteria.[18]

CDNA MICROARRAY ANALYSIS

Cancer cells were isolated by laser capture microdissection. Squamous epithelial cells adjacent to OSCC were isolated from the specimens of nine patients as a normal control. Microarray analyses were performed as described previously.[19]

IMMUNOHISTOCHEMISTRY

Immunohistochemistry was performed according to the standard protocol. For antigen retrieval, the sections were placed in Tris/ethylenediamine tetraacetic acid (EDTA) buffer (10 mM Tris (pH = 9.0) and 1 mM EDTA) and autoclaved at 120°C for 20 min. The primary antibodies were anti-K1 (N-20; Santa Cruz, CA, USA), K2e (Ks2.342.7.1; Progen, Heidelberg, Germany), K4 (EP1599Y; Epitomics, Burlingame, CA, USA), K5 (XM26; Monosan, Uden, Netherlands), K6 (LHK6B; Neomarkers, Lab Vision, Fremont, CA, USA), K7 (RN7; Dako, Glostrup, Denmark), K8 (TS1; Novocastra, Leica Microsystems, Wetzlar, Germany), K9 (Ks9.70/Ks9.216; EuroDiagnostica, Malmö, Sweden), K10 (DE-K10; Neomarkers), K13 (KS-1A3; Novocastra), K14 (LL002; Abcam, Cambridge, MA, USA), K15 (EPR1614Y; Epitomics), K16 (LL025; Neomarkers), K17 (E3; Dako), K18 (DC10; Dako), K19 (EP1580Y; Epitomics), K20 (PW1; Dako) and hair keratins (AE13; Santa Cruz). Antimouse IgG-Alexafluor 594, anti-rabbit IgG-Alexafluor 488 (Invitrogen, Carlsbad, CA, USA), or Envision Dual link kit (Dako) was used as the secondary antibody. Evaluation of the expression was performed by comparing immunoreactivity in the lesion with that in the normal epithelium of the same specimen.

MOLECULAR CLONING OF KERATIN GENES

Human *K4* cDNA (IMAGE: 5453644) was purchased from Geneservice (Cambridge, UK). Human *K5*, *K13*, *K14* and *K17* cDNAs were synthesized by reverse transcriptase–polymerase chain reaction of RNA obtained from the gingiva of a male volunteer. *K4* and *K5* were cloned into pAcGFP1-C2 (Clontech, Mountain View, CA, USA) and *K13*, *K14* and *K17* were cloned into pDsRed-Monomer-N1 (Clontech). *Dominant negative K4* (*dnK4*), lacking the carboxyl terminal region (from S414 to R594), was the deletion construct of *K4*. Details of the cloning procedures will be provided upon request.

CELL CULTURE

HEK293T, Ca9-22 and U2OS cells were cultured in Dulbecco's modified Eagle's medium containing 10% fetal calf serum. Transfections were performed using FuGene6 (Roche Diagnostics, Basel, Switzerland BD Falcon, Franklin Lakes, NJ, USA). To assess the effect of different keratin expression on the cell motility, cells seeded in a Boyden chamber (pore size 8 μm; BD Falcon) were transfected with mock, K13 or K17 plasmid, and cell movement assay was performed as described previously.[20]

Results

CDNA MICROARRAY ANALYSIS OF OSCC

Expression level of the genes encoding each keratin subtype was represented as the mean of the signal

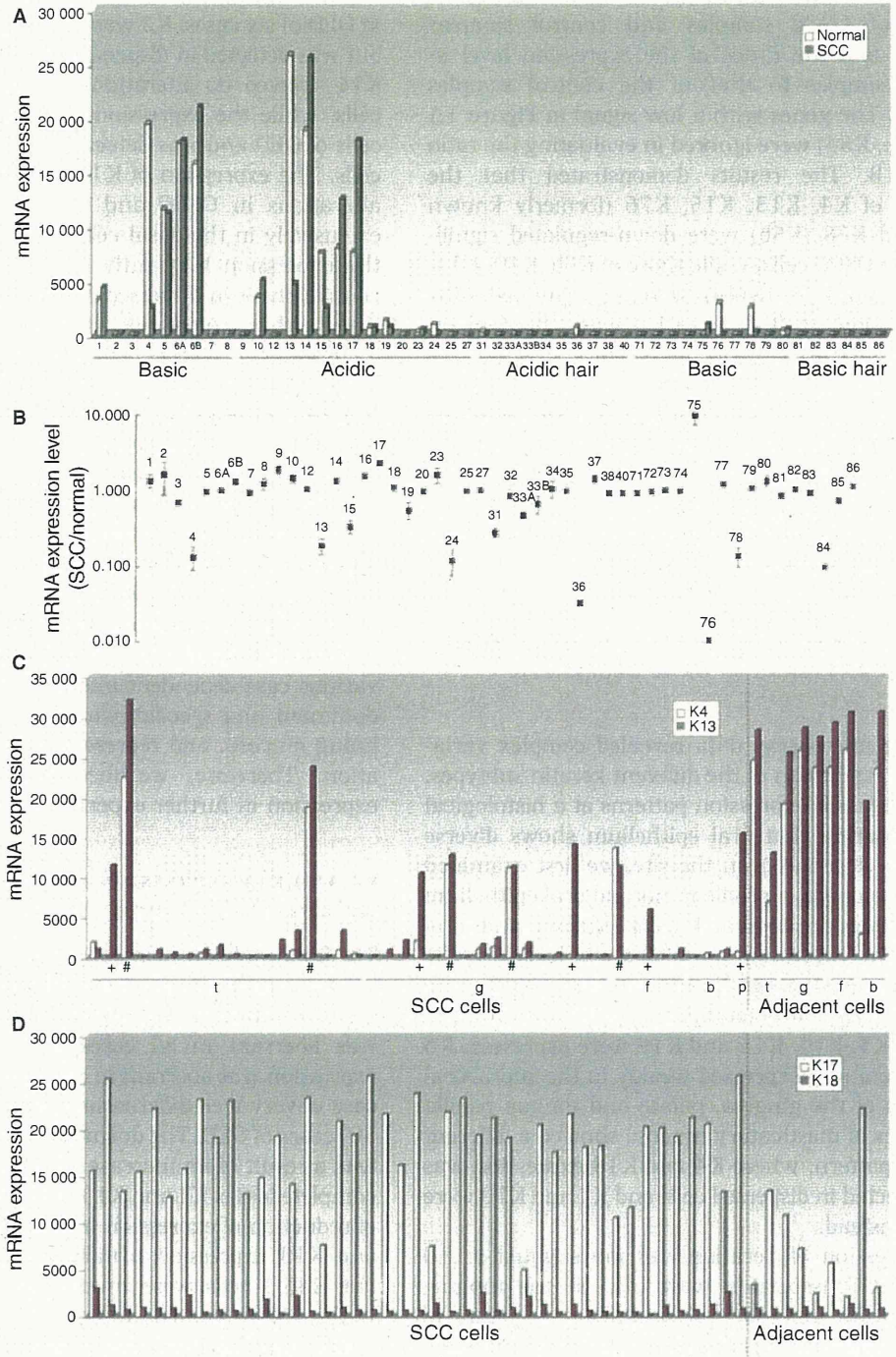

Figure 1. cDNA microarray analysis of oral squamous cell carcinoma (OSCC). **A.** The expressions of each keratin subtype in 43 OSCC samples and nine normal control samples are represented as the mean of the fluorescent signal intensity. Numerals in the horizontal axis denote the keratin subtypes. K1–K8 and K71–K80 are basic epithelial keratins. K9–K27 are acidic epithelial keratins. K31–K40 are acidic hair keratins and K81–K86 are basic hair keratins. Expressions of pseudogenes were omitted. **B.** The expression levels are represented as the ratios of the mean expression in OSCC to that in the normal samples. Error bars denote standard errors. Numerals denote the keratin subtypes. The vertical axis is logarithmic. **C.** The *K4* and *K13* signal intensities of each OSCC that arose in tongue (t), gingiva (g), oral floor (f), buccal mucosa (b) and palate (p). Nine samples to the right are the normal control samples. Crosses denote the cases with considerably retained expression of K13 but not K4. Sharps denote the cases with considerably retained expression of both K4 and K13. **D.** The K17 and K18 signal intensities of each case.

intensities of OSCC samples and control samples (Figure 1A) and the ratios of the expression level in the OSCC samples to that in the control samples (Figure 1B). The genes with a low signal in Figure 1A (for example, *K84*) were ignored in evaluating the ratio in Figure 1B. The results demonstrated that the expressions of K4, K13, K15, K76 (formerly known as K2b) and K78 (K5b) were down-regulated significantly in the OSCC cells, while those of K6b, K10, K14, K16, K17 and K75 (K6hf) were up-regulated. The down-regulation of K4 or K13 was observed in most cases (Figure 1C). Although many studies have reported up-regulation of K8 and K18 during oral carcinogenesis,[5,6,11,16,21,22] OSCC cases with elevated expression of K8, K18 were exceptional and their expression levels were low compared to those of the other keratins (data not shown and Figure 1D). In contrast, significant up-regulation of K17 was observed in most cases (Figure 1D).

IDENTIFICATION OF THE KERATINS WITH ALTERED EXPRESSION PATTERNS IN ORAL NEOPLASTIC LESIONS

Because the microarray data revealed complex variations in the expression of the different keratin subtypes, we examined their expression patterns at a histological level. Considering that oral epithelium shows diverse appearances depending on the site, we first examined the keratin expression profile in normal oral epithelium including tongue, gingiva, buccal mucosa and oral floor. Keratin expression profiles were basically the same throughout the oral cavity. K4 and K13 were expressed strongly in suprabasal cells, whereas in the basal cells, K5, K14, K15 and K19 were expressed. K6 and K16 were also expressed weakly in the suprabasal layer. Parts of the gingiva, palate and tongue papilla that are sites of masticatory mucosa showed a different expression pattern, where K4 and K13 expression was weakly detected in dispersed cells and K1 and K10 were expressed instead.

The expression of keratins was investigated in 10 cases of OSCC associated with OED in the tongue, gingiva, buccal mucosa and oral floor. A panel of keratin expression in a representative case is presented in the Supporting Information. K4 and K13 were significantly down-regulated or almost disappeared in OSCC and OED. K17, which was negative or faintly detected in normal mucosa, was up-regulated in the basal and suprabasal layer of most cases. K1 and K10 were also up-regulated considerably in the suprabasal layers of more than half of OSCC and OED cases. K6 and K16 were up-regulated diffusely in OSCC and also in OED of six cases. K2 was negative in normal mucosa but was detected in dispersed cells of two cases. K5 and K14 showed no alteration of expression in the basal cells, while the expression retained in the suprabasal cells of OED and was detected in virtually all the OSCC cells. The expression of K15 and K19 showed various alterations in OSCC and OED: both were expressed exclusively in the basal cells of normal epithelium but the expression frequently disappeared in OED, either completely or in dispersed cells. In OSCC, K15 and K19 were either completely negative or were detected diffusely or in dispersed cells. The immunohistochemical findings are summarised schematically in Figure 2A. Overall alteration of keratin expression revealed by microarray array analysis and immunohistochemistry is depicted schematically on a genome map (Figure 2B). These results confirmed the microarray data and highlighted relevant keratins to distinguish OED and OSCC from a normal epithelium. Among these, the down-regulation of K4 and K13 expression in lining mucosa was the most consistent. In contrast, expression of the other keratins showed various case-dependent alterations. K4 and K13 are a dominant and specific pair in suprabasal cells of oral lining mucosa, and represent their terminal differentiation. Therefore, we focused upon K4 and K13 expression in further experiments.

K4 AND K13 EXPRESSION ARE DOWN-REGULATED CONSISTENTLY IN OSCC AND OED

The immunohistochemical expression of K4 and K13 in OSCC and OED was investigated in an additional 90 cases (40 OSCCs and 50 OEDs) (Figure 3). K4 expression was aberrant in all cases of OSCC and OED. K13 expression was aberrant in all cases of OSCC, except one case of very well-differentiated SCC, and in 70% (35 of 50) cases of OED. The down-regulation of these proteins was a result of an increase in the number of cells with complete loss of K4 and K13 expression, and not a result of reduction of expression in individual cells. Loss of K4 and K13 expression usually occurred concomitantly, but K4(−) cells were often distributed more broadly in the lesions compared to K13(−) cells (Figure 3A,B). This suggests that the expression of K4 represents the terminal differentiation of oral keratinocytes more strictly than K13, and thus can be used as a more sensitive indicator for its dysregulation. In the OSCC lesions, most of the cancer cells were negative for both K4 and K13 expression (Figure 3A–C), although cancer nests with dispersed K4- and/or K13-positive cells were observed occasionally (Figure 3A). Using immunohistochemistry we investigated the cases in which a

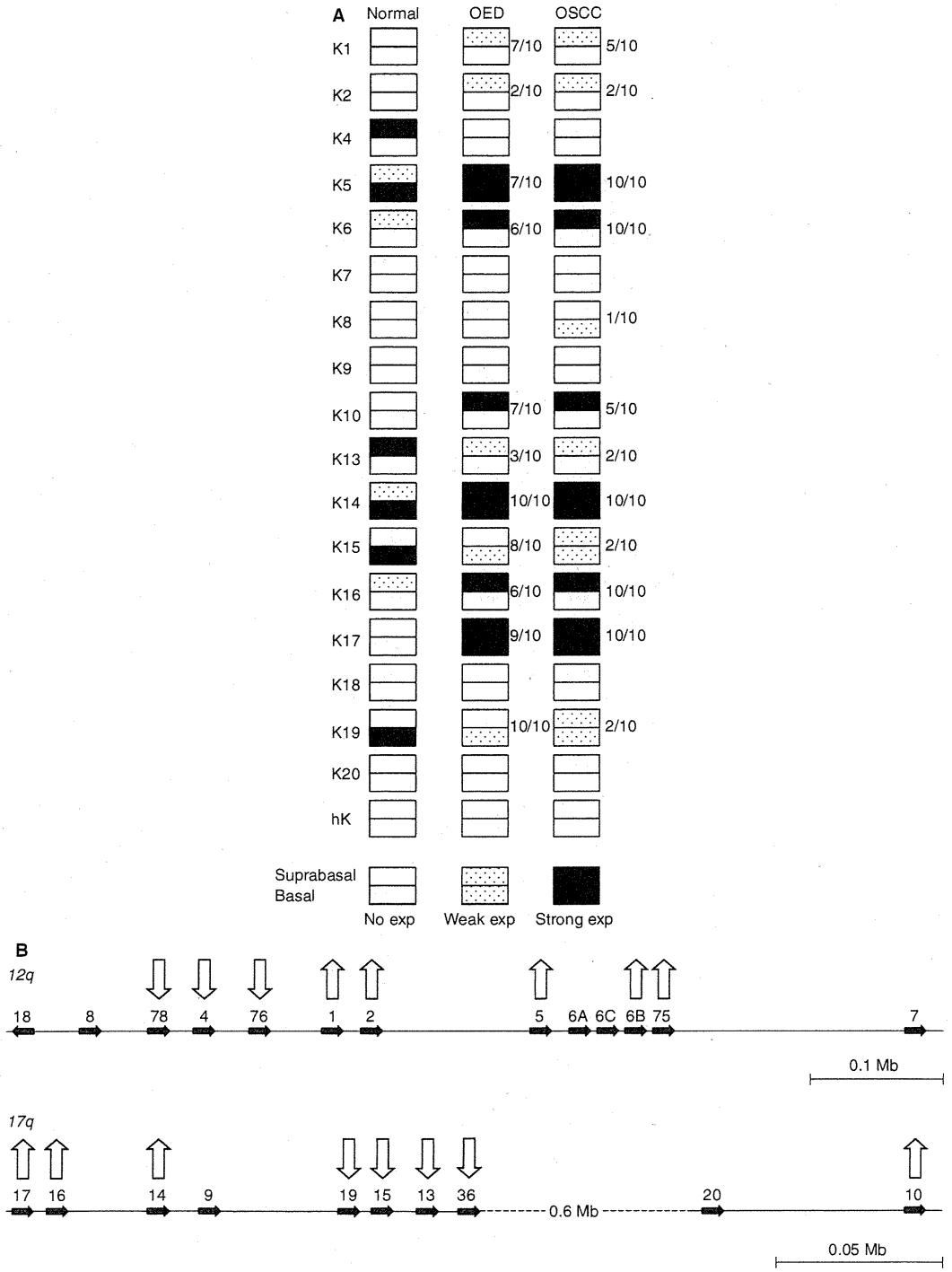

Figure 2. A, Schematic illustration of keratin expression profile in the normal oral mucosa, oral epithelial dysplasia (OED) and oral squamous cell carcinoma (OSCC). The epithelium is divided into basal and the suprabasal compartments and expression is represented by a three-grade evaluation. The black shading (strong expression) represents that the expression was observed strongly in virtually all cells in the positive case. The white shading (no expression) represents that the expression was almost completely negative in all the cases. The dotted shading (weak expression) represents that the expression was detected weakly or partially. The numbers of cases with an altered expression pattern is shown. B, Schematic illustration of the keratin loci, also showing keratins up-regulated (upward arrow) or down-regulated (downward arrow) in OSCC and OED. Only major epithelial keratins and keratins that exhibit significant changes of expression are depicted. The sizes of the genes are not shown.

considerably retained level of K4 or/and K13 expression was indicated by the microarray analysis (marked with '+' or '#', respectively, in Figure 1C), and confirmed that they also showed significant down-regulation of K4 and K13. This minor inconsistency between the microarray analysis and the immunohistochemical examination was due apparently to the sampling from the lesions in which K13-positive (and a few K4-positive) and K13-negative cancer nests coexisted.

In OED, K4 expression was absent or significantly down-regulated in all cases (Figure 3D). Both leucoplakic and erythroplakic lesions showed aberrant K4 expression, regardless of the grade of OED (Figure 3C,D). K13 was also down-regulated significantly in six of 16 cases of mild OED, 19 of 24 cases of moderate OED and all the cases of severe OED. A prominent feature in this observation was that aberrant K4 expression was always observed in a region that exhibited abnormal morphology (dysplasia) and was not observed in epithelium with normal appearance. As the adjacent epithelium usually showed normal K4 expression, the borders of K4 expression were clearly visible. At the periphery of the lesion, the distribution of K4(−) cells could be divided into two patterns:

Type 1
In a majority of cases (38 of 60), a definite border between the K4-positive and -negative regions was observed. The border of K13 expression matched that of K4 expression, although some K13(+) cells often remained in the K4(−) region. In this category, a clear histological demarcation between the normal epithelium and OED was visible, and the histological border coincided with the K4 expression border.

Type 2
In a minority of cases (22 of 60), there was a gradual increase in the number of K4(−) cells towards the centre of the lesion, forming a transition zone with a mixed population of K4-positive and K4-negative cells. In these cases, no distinct histological border was visible.

We examined the coexpression of K4 and K13 in individual cells by immunofluorescent double staining in 10 representative cases of OED. In the normal oral mucosa, suprabasal cells coexpressed both K4 and K13 (Figure 4A). In cases with Type 1 borders, K4(−)K13(−) cells were observed predominantly in the lesion with very few K4(−)K13(+) cells (Figure 4B). In the cases with Type 2 borders, the transition zones comprised mixed populations of K4(+)K13(+), K4(−)K13(−), and K4(−)K13(+) cells. In addition, a few cells with K4(+)K13(−) phenotype, which were never observed in the normal epithelia, were observed (Figure 4C).

PATHOPHYSIOLOGICAL ROLE OF ALTERED KERATIN EXPRESSION

Because the loss of K4 expression was correlated highly with the presence of OED, we hypothesized that aberrant expression of K4 and K13, with concomitant up-regulation of the other keratins, may be one cause of OED. To test this hypothesis, we transfected *K4*, *dnK4* and *K13* in Ca9-22 cells. The keratins were tagged with GFP (K4; green) or RFP (K13; red), allowing direct visualization of keratin filaments. DnK4 could form aggregates with a broad range of keratin subtypes, causing impaired keratin network formation (data not shown). Cotransfection of cognate keratin subtypes (i.e. *K4* and *K13*) resulted in a filamentous arrangement of each keratin subtype (Figure 5A). In contrast, cotransfection of *dnK4* with *K13* resulted in aggregation of both the keratin subtypes and the dnK4-expressing cells decreased in size, were round and showed poor adhesion to the surrounding cells (Figure 5A). These results implied that the impaired formation of a keratin network resulted in alteration in cell shape and attachment.

We next investigated whether K4 or K13 is functional in the absence of its cognate partner using the osteosarcoma cell line U2OS in which no keratins are expressed (data not shown). We transfected U2OS cells

Figure 3. K4 and K13 expression in oral squamous cell carcinoma (OSCC) and dysplasia (OED). **A**, Absence of K4 and K13 expression in well-differentiated squamous cell carcinoma (SCC) of tongue. Most of the cancer cells are negative for both K4 and K13. Some cancer nests contain K4(+) or K13(+) cells in a scattered fashion, where K13(+) cells are observed more than K4(+) cells. **B**, Absence of K4 and K13 expression in early SCC of tongue. The small dysplastic lesion between invasive cancer and normal epithelium shows absent K4 expression, and remaining but down-regulated expression of K13. **C**, A representative case of buccal SCC associated with epithelial dysplasia (OED) that was observed clinically as a mixture of erythroplakia and leucoplakia. High magnification views of selected areas are shown (a–f). The lesion exhibited various histological appearances. (a) Invasive squamous cell carcinoma. (b) Hyperparakeratosis and acanthosis with irregularly elongated rete ridges. (c) Weak keratinization and slightly bulbous rete ridges. (d) Orthokeratinization with minimal architectural and cellular atypia. (e) Weak keratinization with irregular shapes of rete ridges. (f) The periphery of the lesion, revealed by the expression of K4 and K13 as well as by histology. On the left, the affected epithelium is thin with little tendency to keratinization. K4 and K13 were down-regulated in all these lesions (a–f). **D**. Summary of the immunohistochemistry – a number of cases with distinct down-regulation of K4 or K13 are shown.

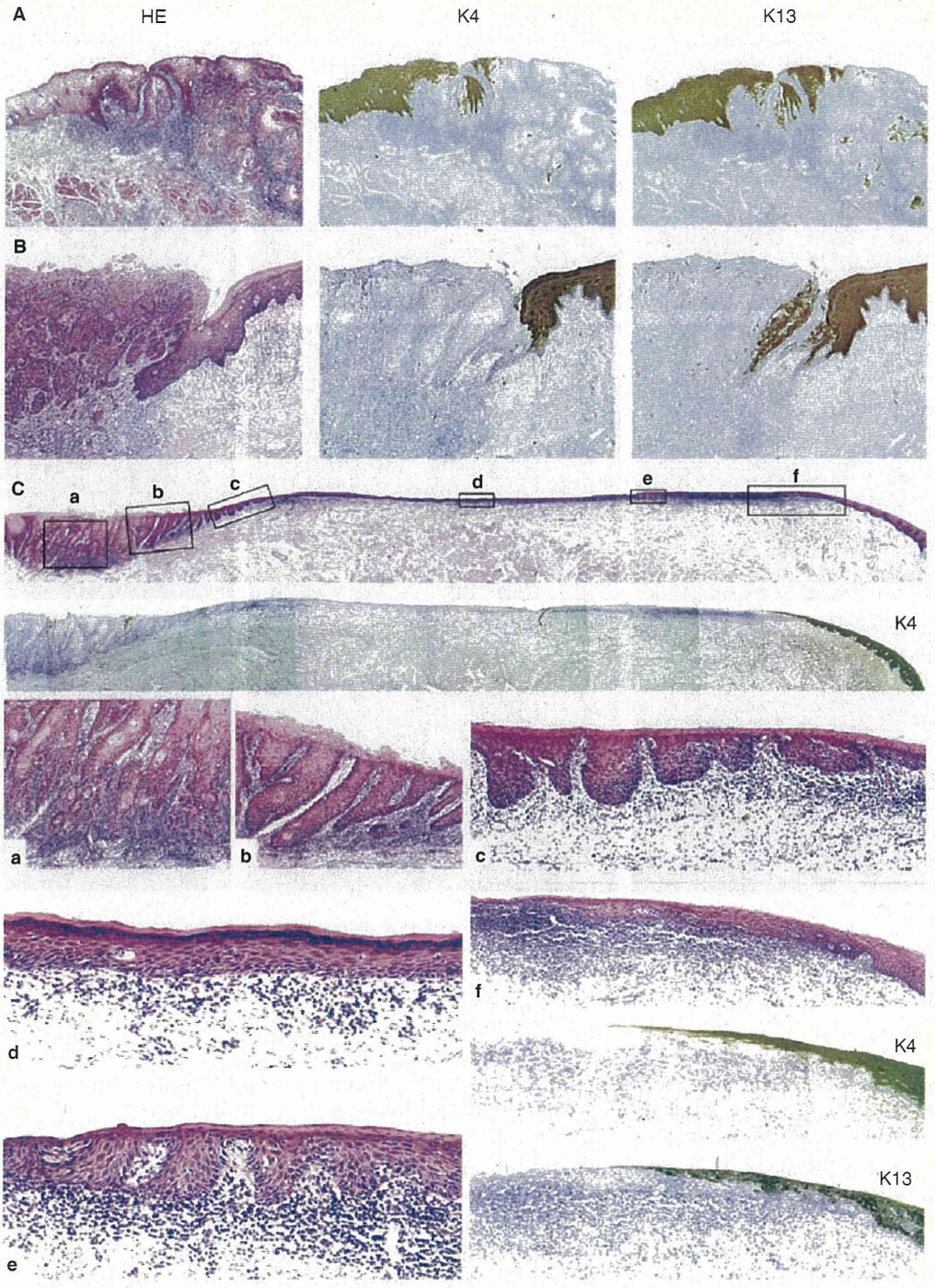

D

	OED			OSCC
	Mild	Moderate	Severe	
K4 ↓	16/16 (100%)	24/24 (100%)	10/10 (100%)	50/50 (100%)
K13 ↓	6/16 (38%)	19/24 (79%)	10/10 (100%)	49/50 (98%)

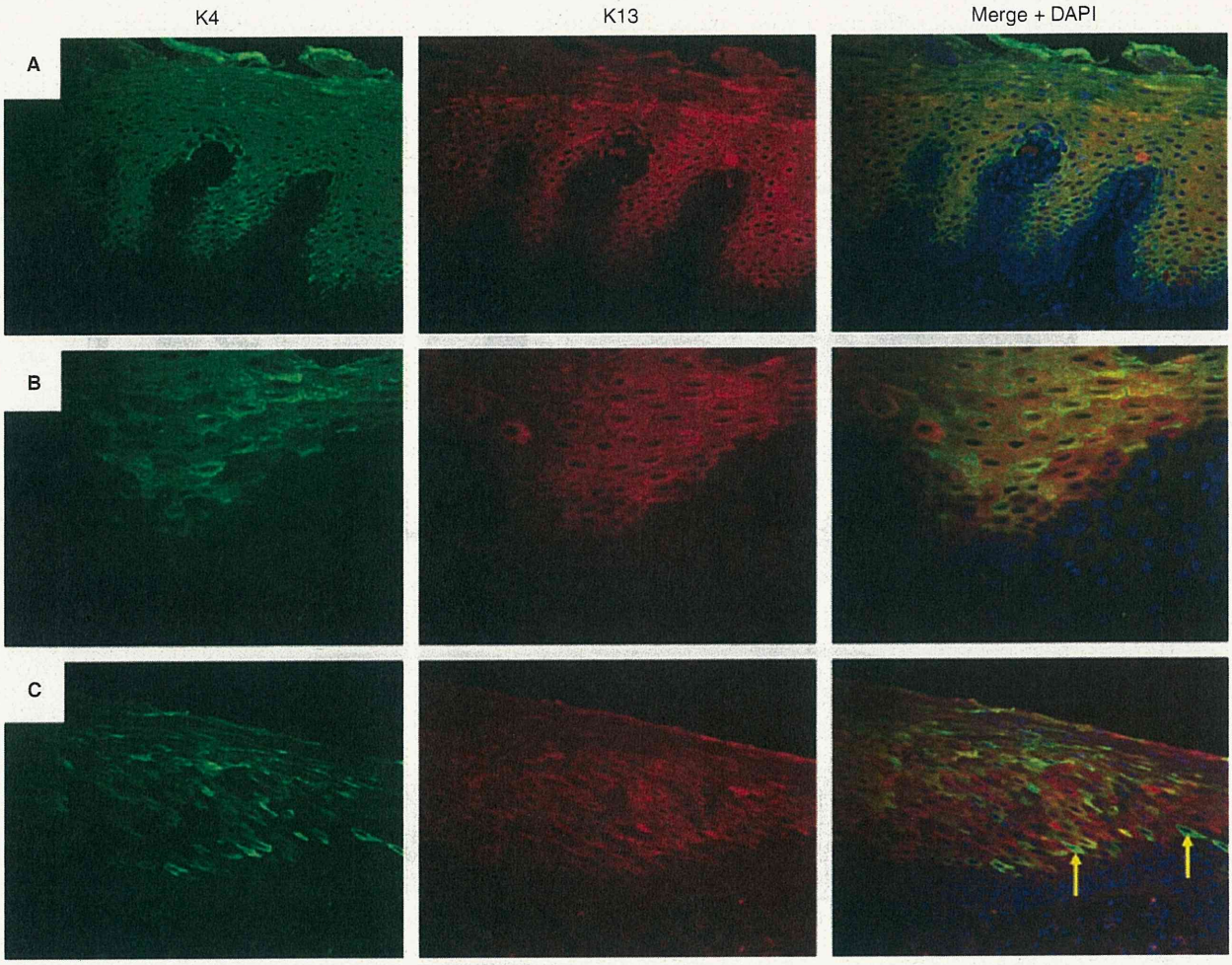

Figure 4. K4 and K13 expression in epithelial dysplasia (OED) revealed by immunofluorescent double staining. **A**, Normal epithelium with K4(+)K13(+) suprabasal cells. **B**, Mild OED with K4(−)K13(+) cells at the periphery of the lesion. **C**, Type 2 border of moderate OED showing a transition zone with a few K4(+)K13(−) cells (arrows).

with the genes of keratin subtypes: *K4*, *K5*, *K13* and *K14* and then examined the distribution of each keratin subtype. As shown in Figure 5B, basic keratins (K4 and K5) exhibited a filamentous network, whereas acidic keratins (K13 and K14) exhibited a diffuse distribution and lacked a filamentous network. This finding suggested that K13 and K14 were not functional in the absence of the basic keratins, although K4 and K5 were somehow integrated into the cytoskeletal network of the U2OS cells. These results suggested that aberrant expression of only one keratin subtype could cause an impaired cytoskeletal network. Nevertheless, a majority of the cells in OED retain relatively normal cytomorphology in the absence of K4 or K13 expression. We assumed that the other keratin subtypes that were induced ectopically could compensate for the loss of K4 or K13.

To test this hypothesis, we cotransfected the U2OS cells with different pairs of these keratins to investigate the mutual interaction of each keratin in the cytoskeletal network formation. Cotransfection with any of the combinations of keratin subtypes, i.e. K4/K13 (a cognate pair of differentiation-related keratins), K5/K14 (a cognate pair of basal cell keratins), K4/K14 and K5/K13, resulted in the formation of similar cytoskeletal network, as observed with the single-gene transfection of K4 or K5 (Figure 5B). This suggested that K5 and K14 could compensate for the function of K4 and K13, respectively, in the cytoskeletal network formation.

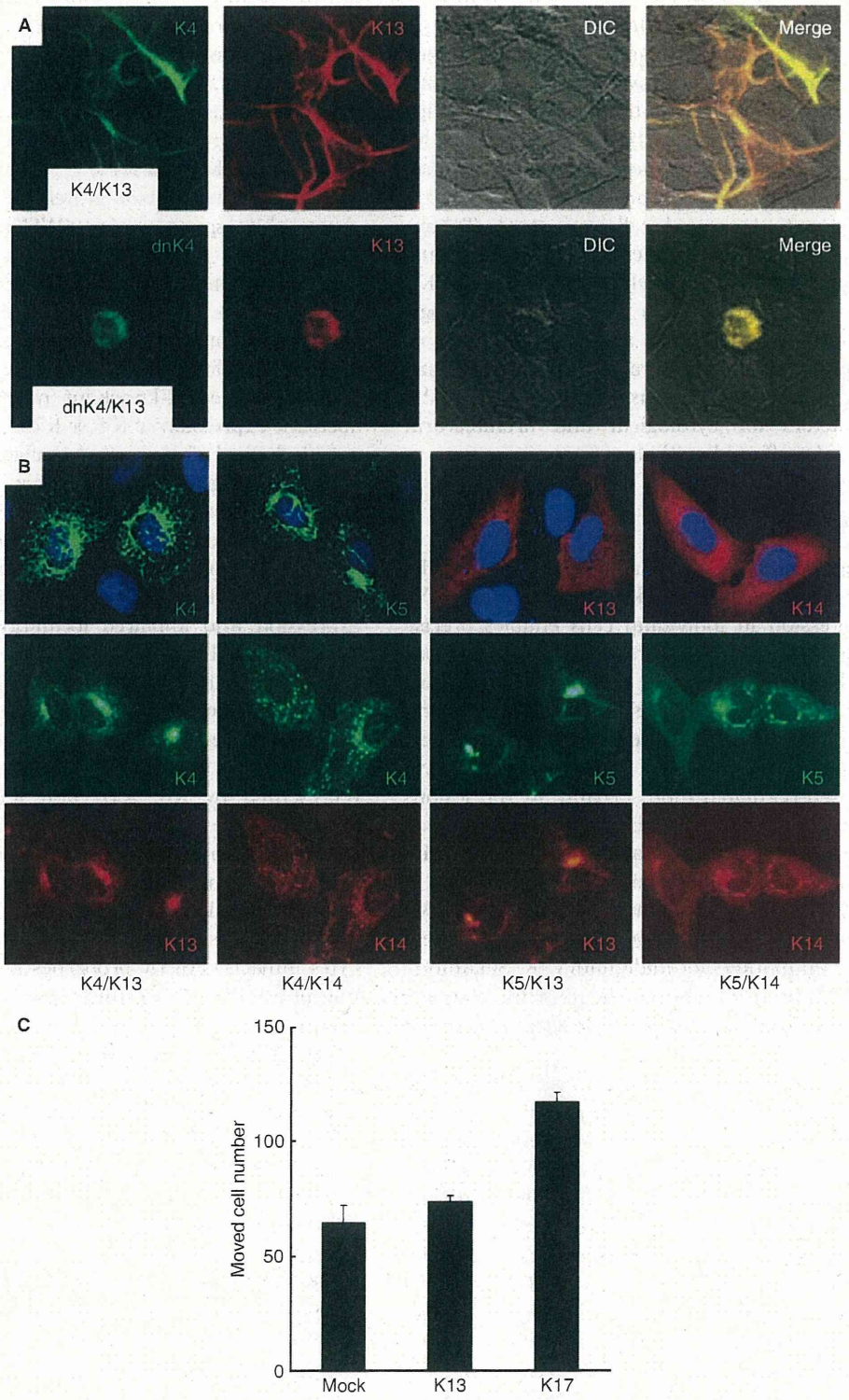

Figure 5. A, Ca9-22 cells cotransfected with *K4* or *dominant negative K4* (*dnK4*) and *K13*, tagged with GFP and RFP, respectively. B, K4/K14 or K5/K13 pairs are incorporated into the cytoskeletal networks similar to K4/K13 and K5/K14 pairs. U2OS cells were transfected with *GFP-K4*, *GFP-K5*, *K13-RFP* and *K14-RFP* at the indicated combination. C, Cell movement assay. HEK293T cells were transfected with a mock, K13 or K17 plasmid. After 24 h, the cells that moved to the external plate were counted. The results are the mean value of a triplicate experiment.

Finally, we examined the effect of keratin subtype expression on cell movement using a Boyden chamber assay. K17-transfected cells showed increased motility compared to mock- or K13-transfected cells (Figure 5C). This result implies that induction of K17 expression, which occurs in most cases of OSCC and OED, may lead to architectural alteration of the epithelium due to increased cell movement. Taking these results together with the *in situ* observations, demonstrating that the epithelia with aberrant K4 or/and K13 expression always exhibited morphological alterations, we assume that aberrant expression of these differentiation-related keratins and concomitant up-regulation of other keratins may be one of the causative factors for cytological and architectural alteration of the affected epithelium.

Discussion

We have demonstrated that features of K4 and K13 render them as relevant biomarkers for OED and OSCC. Distinct expression in individual cells enables precise and reliable evaluation; they are down-regulated consistently in OSCC and OED; and, because these keratins are major keratin pairs in the suprabasal cells of oral epithelium, their aberrant expression indicates abnormal terminal differentiation. As K4 was more sensitive and was down-regulated more broadly in the lesions than K13, we think that K4 is the first choice as a marker for dysregulation of oral epithelial differentiation. We compared the expression of K4 with that of Ki67 and TP53, and found that the usability of K4 was comparable to or even more sensitive than these commonly used markers for malignancy (K. Sakamoto, unpublished data). Combined usage of these markers for different cellular properties would facilitate more precise diagnosis.

OEDs are experienced commonly as a white patch (leukoplakia) or a red lesion (erythroplakia). Leukoplakia could be divided roughly into two groups on the basis of their keratin profiles. One was a K1(+)K10(+) lesion, in which the expressions of K4 and K13 were substituted for by their epidermal counterparts, K1 and K10, respectively, and the lesion exhibited an orthokeratotic appearance. The other was a K1(−)K10(−) lesion that typically showed hyperparakeratosis, although this keratosis was not achieved by original K4 and K13 pairs but by the other up-regulated keratins such as K5, K6, K14, K16, and especially K17. When little expression of the differentiation-related keratins was induced, the lesion led to poor development of the prickled cell layer, exhibiting an erythroplakic appearance (unpublished data). These are examples of the direct correlation between alteration of keratin expression and changes in the epithelial morphology. In any case, down-regulation of K4 and K13 seemed essential as we never observed the other keratins up-regulation in the presence of normal expression of K4 and K13.

Missense mutations in either *K4* and *K13* genes can cause white sponge nevus (WSN).[23,24] Furthermore, *K4* knockout mice show a cellular phenotype that resembles epithelial dysplasia in humans, including hyperkeratosis, atypical nuclei and cell degeneration.[25] Although commonly experienced OED usually show somewhat different histological features from that of WSN and the K4-knockout mice, these imply that aberrant expression of K4 or K13 may lead possibly to morphological change of the affected epithelium. We have demonstrated that regions with aberrant K4 and K13 expression coincide with altered epithelial morphology, including the concurrent formation of a histological border with a K4-expression border. Cell culture experiments suggest that aberrant keratin expression and impaired formation of a cytoskeletal network could cause changes in cell shape. This may not be a dominant factor for alteration of the whole epithelial morphology, because other keratins are usually induced in order to compensate for the absence of the original keratins. Rather, increased cell motility represented by K6, K16 and K17 expression may associate with architectural alterations. These keratins are induced robustly in a hyperproliferative epithelium after injury, and their presence correlates with changes in the morphology of epithelial cells at a wound edge.[26] Forced expression of K16 in progenitor skin keratinocytes impacts directly properties such as adhesion and migration.[27] Our results demonstrate that forced expression of K17 leads to increased cell migration. Altogether, we assume that alteration of keratin subtype expression is one of the factors that underlie cytological and architectural alterations observed in OED and OSCC. If so, keratin profiling is not only a practical but also a rational aid for pathological diagnosis.

The upstream factors that initiate changes in keratin subtype expression in the oral mucosa are currently unknown. We examined immunohistochemically several factors that reportedly regulate keratinocyte differentiation, such as p63, FoxN1, AKT, ERK, FAK and integrins, but none showed a correlation with K4 and K13 expression (data not shown). A high correlation between K4 and K13 expression patterns suggests the presence of a common mechanism to regulate their transcription, but little sequence homology was found in their promoter regions (data not

shown). The well-coordinated regulation of multiple keratin expression may be associated with the unique genome organization of keratin genes. Basic and acidic keratin genes, except *K18* (which locates on *12q* back to back with K8), are aligned tandemly on *12q* and *17q*, respectively, and this genomic organization is evolutionarily well conserved. Our comprehensive keratin profiling reveals that each of the up-regulated and down-regulated keratins in OSCC and OED is clustered on the genome (Figure 2B). This implies that the epigenetic status of keratin loci may be important for the selective expression of specific repertoires of keratins. In this sense, analysis of methylation states in the keratin loci would be an interesting future project for understanding the coordinated expression of different keratin subtypes.

In conclusion, our study demonstrated that aberrant expression of K4 and K13, which are differentiation-related keratins in oral keratinocytes, is the most essential feature observed in OSCC and OED.

Acknowledgements

This work was supported by a grant-in-aid from the Japanese Ministry of Education, Culture, Sports, Science and Technology (KAKENHI 21592320). The authors thank Miwako Hamagaki and Kiyoko Nagumo for technical assistance and undergraduate students Yuhei Ikeda and Ryushiro Sugita for their contributions to this study.

References

1. Moll R, Divo M, Langbein L. The human keratins: biology and pathology. *Histochem. Cell Biol.* 2008; **129**; 705–733.
2. Crowe DL, Milo GE, Shuler CF. Keratin 19 downregulation by oral squamous cell carcinoma lines increases invasive potential. *J. Dent. Res.* 1999; **78**; 1256–1263.
3. Farrar M, Sandison A, Peston D, Gailani M. Immunocytochemical analysis of AE1/AE3, CK 14, Ki-67 and p53 expression in benign, premalignant and malignant oral tissue to establish putative markers for progression of oral carcinoma. *Br. J. Biomed. Sci.* 2004; **61**; 117–124.
4. Fillies T, Werkmeister R, Packeisen J *et al.* Cytokeratin 8/18 expression indicates a poor prognosis in squamous cell carcinomas of the oral cavity. *BMC Cancer* 2006; **6**; 10.
5. Gires O, Mack B, Rauch J, Matthias C. CK8 correlates with malignancy in leukoplakia and carcinomas of the head and neck. *Biochem. Biophys. Res. Commun.* 2006; **343**; 252–259.
6. Matthias C, Mack B, Berghaus A, Gires O. Keratin 8 expression in head and neck epithelia. *BMC Cancer* 2008; **8**; 267.
7. Ogden GR, Lane EB, Hopwood DV, Chisholm DM. Evidence for field change in oral cancer based on cytokeratin expression. *Br. J. Cancer* 1993; **67**; 1324–1330.
8. Ohkura S, Kondoh N, Hada A *et al.* Differential expression of the keratin-4, -13, -14, -17 and transglutaminase 3 genes during the development of oral squamous cell carcinoma from leukoplakia. *Oral Oncol.* 2005; **41**; 607–613.
9. Su L, Morgan PR, Lane EB. Keratin 14 and 19 expression in normal, dysplastic and malignant oral epithelia. A study using *in situ* hybridization and immunohistochemistry. *J. Oral Pathol. Med.* 1996; **25**; 293–301.
10. Toyoshima T, Vairaktaris E, Nkenke E, Schlegel KA, Neukam FW, Ries J. Cytokeratin 17 mRNA expression has potential for diagnostic marker of oral squamous cell carcinoma. *J. Cancer Res. Clin. Oncol.* 2008; **134**; 515–521.
11. Xu XC, Lee JS, Lippman SM, Ro JY, Hong WK, Lotan R. Increased expression of cytokeratins CK8 and CK19 is associated with head and neck carcinogenesis. *Cancer Epidemiol. Biomarkers Prev.* 1995; **4**; 871–876.
12. Yanagawa T, Yoshida H, Yamagata K *et al.* Loss of cytokeratin 13 expression in squamous cell carcinoma of the tongue is a possible sign for local recurrence. *J. Exp. Clin. Cancer Res.* 2007; **26**; 215–220.
13. Zhong LP, Chen WT, Zhang CP, Zhang ZY. Increased CK19 expression correlated with pathologic differentiation grade and prognosis in oral squamous cell carcinoma patients. *Oral Surg. Oral Med. Oral Pathol. Oral Radiol. Endod.* 2007; **104**; 377–384.
14. Depondt J, Shabana AH, Sawaf H, Gehanno P, Forest N. Cytokeratin alterations as diagnostic and prognostic markers of oral and pharyngeal carcinomas. A prospective study. *Eur. J. Oral Sci.* 1999; **107**; 442–454.
15. Fillies T, Jogschies M, Kleinheinz J, Brandt B, Joos U, Buerger H. Cytokeratin alteration in oral leukoplakia and oral squamous cell carcinoma. *Oncol. Rep.* 2007; **18**; 639–643.
16. Ogden GR, Chisholm DM, Adi M, Lane EB. Cytokeratin expression in oral cancer and its relationship to tumor differentiation. *J. Oral Pathol. Med.* 1993; **22**; 82–86.
17. Vaidya MM, Borges AM, Pradhan SA, Bhisey AN. Cytokeratin expression in squamous cell carcinomas of the tongue and alveolar mucosa. *Eur. J. Cancer B Oral Oncol.* 1996; **32B**; 333–336.
18. Barnes L, Eveson J, Reichart P, Sidransky D. Epithelial precursor lesions. *World Health Organization classification of tumours. Pathology and genetics. Head and neck tumours.* Geneva, Switzerland: WHO Press, 2005; 177–180.
19. Tomioka H, Morita K, Hasegawa S, Omura K. Gene expression analysis by cDNA microarray in oral squamous cell carcinoma. *J. Oral Pathol. Med.* 2006; **35**; 206–211.
20. Bonifacino JS, Dasso M, Harford JB, Lippincott-Schwartz J, Yamada KM. *Current protocols in cell biology*. Hoboken, NJ, USA: John Wiley and Sons, Inc., 2007.
21. Su L, Morgan PR, Lane EB. Protein and mRNA expression of simple epithelial keratins in normal, dysplastic, and malignant oral epithelia. *Am. J. Pathol.* 1994; **145**; 1349–1357.
22. Zhong LP, Zhao SF, Chen GF, Ping FY, Xu ZF, Hu JA. Increased levels of CK19 mRNA in oral squamous cell carcinoma tissue detected by relative quantification with real-time polymerase chain reaction. *Arch. Oral Biol.* 2006; **51**; 1112–1119.
23. Richard G, De Laurenzi V, Didona B, Bale SJ, Compton JG. Keratin 13 point mutation underlies the hereditary mucosal epithelial disorder white sponge nevus. *Nat. Genet.* 1995; **11**; 453–455.
24. Rugg EL, McLean WH, Allison WE *et al.* A mutation in the mucosal keratin K4 is associated with oral white sponge nevus. *Nat. Genet.* 1995; **11**; 450–452.
25. Ness SL, Edelmann W, Jenkins TD, Liedtke W, Rustgi AK, Kucherlapati R. Mouse keratin 4 is necessary for internal epithelial integrity. *J. Biol. Chem.* 1998; **273**; 23904–23911.

26. Mazzalupo S, Wong P, Martin P, Coulombe PA. Role for keratins 6 and 17 during wound closure in embryonic mouse skin. *Dev. Dyn.* 2003; **226**; 356–365.
27. Wawersik M, Coulombe PA. Forced expression of keratin 16 alters the adhesion, differentiation, and migration of mouse skin keratinocytes. *Mol. Biol. Cell* 2000; **11**; 3315–3327.

Supporting Information

Additional Supporting Information may be found in the online version of this article:

Figure S1. A panel indicating the major keratin expression pattern in a case of oral squamous cell carcinoma of tongue.

Please note: Wiley-Blackwell are not responsible for the content or functionality of any supporting materials supplied by the authors. Any queries (other than missing material) should be directed to the corresponding author for the article.